SYNTHESIS OF DRUG LOADED pH SENSITIVE ALBUMIN NANOPARTICLES

A Thesis Submitted to
The Graduate School of Engineering and Science of
İzmir Institute of Technology
in Partial Fulfillment of the Requirements for the Degree of

MASTER OF SCIENCE

in Materials Science and Engineering

by
Eda ARGITEKİN

December 2023
İZMİR

We approve the thesis of **Eda ARGITEKİN**

Examining Committee Members:

Prof. Dr. Yaşar AKDOĞAN
Department of Materials Science and Engineering, İzmir Institute of Technology

Asst. Prof. Dr. Onur BÜYÜKÇAKIR
Department of Chemistry, İzmir Institute of Technology

Asst. Prof. Dr. Muhammed ÜÇÜNCÜ
Department of Basic Pharmaceutical Sciences, İzmir Kâtip Çelebi University

09 December 2023

Prof. Dr. Yaşar AKDOĞAN
Supervisor, Department of
Materials Science and Engineering,
İzmir Institute of Technology

Assoc. Prof. Dr. Umut ADEM
Co-Supervisor, Department of
Materials Science and Engineering,
İzmir Institute of Technology

Prof. Dr. Yaşar AKDOĞAN
Head of the Department of
Materials Science and Engineering

Prof. Dr. Mehtap EANES
Dean of the Graduate School of
Engineering and Sciences

ACKNOWLEDGEMENTS

I would like to express my special thanks of gratitude to my advisor Prof. Dr. Yaşar Akdoğan for his motivation, patience, sharing his knowledge and experience with me throughout my master's program. Thanks to him, I gained a scientific vision that improve my study. I am sure that his inputs during my study will be useful throughout my career.

I would also like to thank Asst. Prof. Dr. Onur Büyükçakır and Asst. Prof. Dr. Muhammed Üçüncü for participating as a thesis committee and providing helpful feedback and suggestions.

I am also grateful to Dr. Gülçin Çakan-Akdoğan and M.Sc. Esra Ersöz-Gülseven from Izmir Biomedicine and Genome Center (IBG) for cell uptake and cell viability experiments and contribution to these parts with fruitful discussion. I would like to thank IZTECH Center for Materials Research and IZTECH Biotechnology and Bioengineering Research Center. Also, I would like to thank Prof. Dr. Mustafa Muammer Demir to allow me to do DLS analyses in their laboratory.

I would like to thank TÜSEB (11975) program for supporting me during the project.

I am extremely grateful to my labmates Sümeyra Çiğdem Sözer and Cansu Karpuzcu, friends in Materials Science and Engineering Department Tuğçe Egesoy, Merve Karakaya, Tuğçe Irmak and Ezgi Oğur for their valuable advices, sharing their knowledge, emotional support, invaluable friendships throughout my master of thesis. Without their encouragement and motivation, I would not have been able to complete this journey. Also, I am grateful to my childhood friends, Begüm Kılıçarslaner, Simay Oruç and Süleyman Keskinel for their patience and emotional support during my master of thesis.

I appreciate for having unconditioned support of my family, Dilek Argıtekin and Serdar Argıtekin. I am very grateful to have my sister Ece İnan and brother-in-law Erhan İnan for their emotional support. Special thanks to my niece and nephew, Irmak İnan and Kaan İnan for giving me strength and improving my morale with their presence

ABSTRACT

SYNTHESIS OF DRUG LOADED pH SENSITIVE ALBUMIN NANOPARTICLES

Serum albumin-based nanoparticles (NPs) are commonly used for drug delivery due to their stability, biodegradability, ease of particle size control and no toxicity. In this study, bovine serum albumin (BSA) was functionalized with catechol-containing dopamine (D) to synthesize D-BSA NPs using pH responsive catechol-metal coordination bonds. Instead of using glutaraldehyde, V(III) ion was used as a cross-linker for synthesizing NPs. Catechol-V(III) coordination bonds provided pH responsive NPs due to their different stoichiometry of catechol-metal complexes (e.g. mono-, bis- or tris-) at different pH values.

For the synthesis of D-BSA NPs, desolvation method was used with acetone as desolvating agent. Uniformly sized NPs were synthesized with an average of 294 nm with a PDI value of 0.15. Doxorubicin is loaded to NPs with a 15:1 DOX:D-BSA molar ratio. DOX encapsulation efficiency and drug loading capacity of D-BSA NPs were found to be 98% and 10%, respectively. Conversion to bis- and/or mono- catechol-V(III) complexes in acidic medium resulted in degradation of NPs and rapid release of the loaded doxorubicin (DOX). DOX releases reached to 51, 76 and 95% at pH values 7.4, 5.5 and 4.2, respectively at the end of 80 hours.

Furthermore, the cytotoxic effects of prepared D-BSA NPs, in comparison to free DOX were studied with MCF-7 cells. Increasing D-BSA concentrations up to 0.2 mg/mL did not affect the cell viability, significantly. But, upon cell (MCF-7) uptake in vitro, DOX-loaded D-BSA NPs and free DOX reduced cell viability by 75% and 20% in 24 hours, respectively.

ÖZET

İLAÇ YÜKLÜ pH DUYARLI ALBÜMİN NANOPARÇACIKLARIN SENTEZİ

Serum albümin temelli nanoparçacıkların kararlı olmaları, biyolojik olarak parçalanabilir özellikte olmaları, parçacık boyutlarının kolay kontrol edilebilmesi ve toksik olmamaları nedeniyle ilaç taşınımı çalışmalarında yaygın olarak kullanılmaktadırlar. Bu çalışmada, pH duyarlı katekol-metal koordinasyon bağlarından faydalanılarak elde edilen nanoparçacıkları (NP) sentezlemek için sığır serum albümini (BSA), katekol içeren dopamin (D) ile fonksiyonelleştirilmiştir. Nanoparçacıkların sentezlenmesi için çapraz bağlayıcı olarak glutaraldehit yerine V(III) iyonu kullanılmıştır. Katekol-V(III) koordinasyon bağları, farklı pH değerlerinde farklı stokiyometriler (örneğin mono-, bis- veya tris-) oluşturması nedeniyle pH'a duyarlı nanoparçacıkların (D-BSA NPs) sentezlenmesini sağlamıştır.

Bu çalışmada, desolvasyon yöntemi ile NP sentezi yapılmış ve desolvasyon ajanı olarak da aseton kullanılmıştır. Ortalama 294 nm boyutlu 0.15 PDI değerinde NP'ler oluşmuştur. Kanser ilacı olan doksorubisin (DOX), nanoparçacığa 15:1 DOX:D-BSA mol oranı ile yüklenmiştir. D-BSA NP'lerin DOX enkapsülasyon verimi ve ilaç yükleme kapasitesi sırasıyla %98 ve %10'dur. Asidik ortamda, bis- ve/veya mono-katekol-V(III) komplekslerine dönüşerek NP'ların bozulmasına ve yüklü doksorubisinin (DOX) hızlı salınmasını sağlamıştır. 80 saat sonunda, DOX salınımları sırasıyla 7.4, 5.5 ve 4.2 pH değerlerinde %51, %76 ve %95'e ulaşmıştır.

Ayrıca, hazırlanan D-BSA NP'lerin sitotoksik etkileri, serbest DOX ile karşılaştırmalı olarak MCF-7 hücreleri ile çalışılmıştır. D-BSA konsantrasyonlarının 0.2 mg/mL'ye kadar artırılması hücre canlılığında önemli bir değişime sebep olmamıştır. Ayrıca, in vitro hücre (MCF-7) alımı sonrasında, DOX yüklü D-BSA NP'ler ve serbest DOX 24 saat içinde hücre canlılığını sırasıyla %75 ve %20 oranında azaltmıştır.

TABLE OF CONTENTS

LIST OF FIGURES

Figure **Page**

Figure **Page**

Figure **Page**

LIST OF TABLES

Table **Page**

CHAPTER 1

INTRODUCTION

1.1. Nanocarriers

In cancer treatment, chemotherapy is mainly used as a solution. However, this technique causes various side effects due to toxic effect of the drug to the healthy cells. (Chamundeeswari et al., 2019). In recent years, developing new drug delivery agents to improve cancer treatment is one of the important topics for scientific community. For this aim, carrier systems especially nanocarriers have been introduced which are target-specific delivery systems without losing drug activity and minimized adverse effects of drugs (Karewicz, 2014; Din et al., 2017).

There are some properties which a carrier system should provide for drug delivery. Primarily, designed nanocarrier system should be biocompatible, non-toxic and biodegradable to be safely used in human body (Karewicz, 2014). Also, nanocarriers should recognize cancerous cells, protect drug molecules from degradation, and be able to release the drug in the target cells at a controllable rate to achieve desired pharmacological response (Manju and Sreenivasan, 2010).

Physiochemical properties of nanocarriers are able to be modified in terms of chemical composition, size, shape, structure, morphology, and surface properties to enhance their activity with decreasing side effects (Sun et al., 2014). Using nanocarriers, poorly soluble drugs in water can be delivered and drug can be protected better from harsh environments such as highly acidic or enzymatic conditions in the body. Also, their target-specific and/or stimuli-responsive nature can improve delivery of drugs in a cell. It improves treatment efficacy and co-delivery of different types of drugs and/or diagnostic agents to achieve combination therapy. It can provide multifaceted approach to treatment (Sun et al., 2014).

Nanocarriers are mainly classified as organic, inorganic and composite materials (Figure 1.1). Inorganic nanoparticles are commonly prepared from 3 different types of materials; noble metals such as gold, copper and silver; magnetic nanoparticles such as superparamagnetic materials with large magnetic moments in a magnetic field made from

Ni, Co, Fe, Fe_3O_4, and FePt; and fluorescent nanoparticles such as SiO_2, quantum dots etc. (Zhang et al., 2014). They exhibit specific nanoscale physical properties such as high mechanical strength and resistant to enzymatic degradation in biological fluids (Croissant et al., 2017). However, due to their heavy metal content, inorganic nanocarriers may cause long-term health issues (Chamundeeswari et al., 2019). Organic nanocarriers are carbon-based materials loaded drugs are often trapped or bound within the matrix (López-Dávila et al., 2012). Solid lipid nanocarriers, polymeric nanocarriers, liposomes, dendrimers, micelles and viral nanocarriers are classified as organic materials. Due to their versatility in nature and less/no toxicity, they are more favorable compared to inorganic nanocarriers. Also, organic nanocarriers are able to conjugate a variety of drugs as well (Chamundeeswari et al., 2019). For the composite nanocarriers, several materials that can be inorganic or organic are composed by the combination of particles with different component, such as core-shell or hybrid structures. By this strategy, limited properties of single-component structures are resolved such as solubility and biocompatibility (Gessner and Neundorf, 2020).

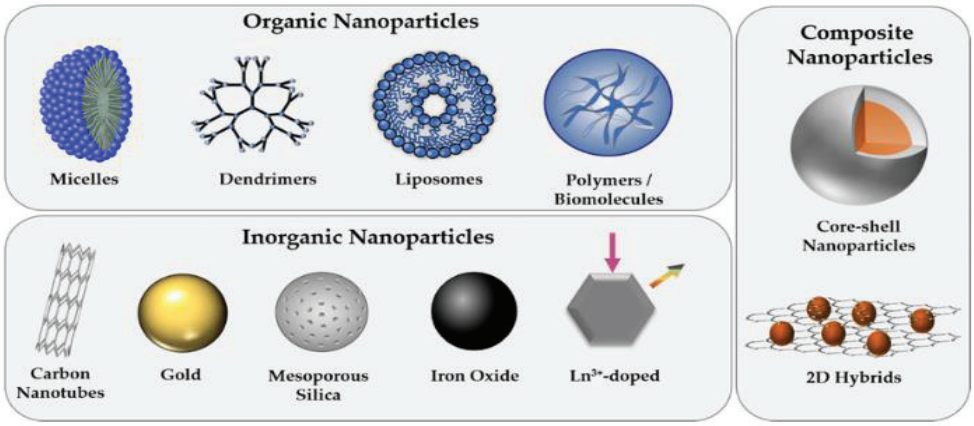

Figure 1.1. Overview of commonly used nanoparticle (NP) types, classified as organic, inorganic, or composite structures (Gessner and Neundorf, 2020).

For cancer treatment, many different types of nanocarriers are formulated for commercial usage. Their commercial names with therapeutic applications are shown as a list in Table 1.1. These formulations are approved by the Food and Drug Administration (FDA) and/or the European Medicines Agency (EMA). The first nanocarrier for cancer treatment was developed by using PEGylated liposomes for doxorubicin encapsulation (Doxil®, Caelyx®). Sterically stabilized liposomes Doxil® composed of phospholipids, cholesterol, and a lipopolymer (PEG) and has particles size less than 120 nm. Doxil® was

approved by FDA in 1995. Its application area is treatment of breast and ovarian cancers (Anselmo and Mitragotri, 2019). Abraxane® is an albumin-conjugated nanoparticle with 130 nm size. It was approved in 2005 by FDA and in 2008 by EMA. It was developed for delivery of paclitaxel and used in non-small lung cancer and metastatic breast cancer treatment (Karami et al., 2020).

Table 1.1. Cancer nanoparticle medicines (Anselmo and Mitragotri, 2019).

Name	Particle type/drug	Approved application	Approval (year)	Investigated application/ indication
VYXEOS CPX-351 (Jazz Pharmaceuticals	Liposomal formulation of cytarabine: daunorubicin (5:1 M ratio)	Acute myeloid leukemia	FDA (2017) EMA (2018)	Various leukemias
ONPATTRO Patisiran ALN-TTR02 (Alnylam Pharmaceuticals)	Lipid nanoparticle RNAi for the knockdown of disease-causing TTR protein	Transthyretin (TTR)-mediated amyloidosis	FDA (2018) EMA (2018)	Transthyretin (TTR)-mediated amyloidosis
Doxil Caelyx (Janssen)	Liposomal doxorubicin (PEGylated)	Ovarian cancer (secondary to platinum based therapies) HIV-associated Kaposi's sarcoma (secondary to chemotherapy) Multiple myeloma (secondary)	FDA (1995) EMA (1996)	Various cancers including: solid malignancies, ovarian, breast, leukemia, lymphomas, prostate, metastatic, or liver
DaunoXome (Galen)	Liposomal daunorubicin (non-PEGylated)	HIV-associated Kaposi's sarcoma (primary)	FDA (1996)	Various leukemias
Myocet (Teva UK)	Liposomal doxorubicin (non-PEGylated)	Treatment of metastatic breast cancer (primary)	EMA (2000)	Various cancers including: breast, lymphoma, or ovarian
Abraxane (Celgene)	Albumin-particle bound paclitaxel	Advanced non-small cell lung cancer (surgery or radiation is not an option) Metastatic breast cancer (secondary) Metastatic pancreatic cancer (primary)	FDA (2005) EMA (2008)	Various cancers including: solid malignancies, breast, lymphomas, bladder, lung, pancreatic, head and neck, prostate, melanoma, or liver
Marqibo (Spectrum)	Liposomal vincristine (non-PEGylated)	Philadelphia chromosomenegative acute lymphoblastic leukemia (tertiary)	FDA (2012)	Various cancers including: Lymphoma, brain, leukemia, or melanoma
MEPACT (Millennium)	Liposomal mifamurtide (non-PEGylated)	Treatment for osteosarcoma (primary following surgery)	EMA (2009)	Osteosarcomas
Onivyde MM-398 (Merrimack)	Liposomal irinotecan (PEGylated)	Metastatic pancreatic cancer (secondary)	FDA (2015)	Various cancers including: solid malignancies, breast, pancreatic, sarcomas, or brain

1.2. Serum Albumin as Nanocarrier Systems

Biological polymeric compounds named as biopolymer nanocarriers are commonly used for drug delivery due to their biocompatibility, antibacterial properties, photoprotection, and active surface functionality (Vodyashkin et al., 2022). Proteins and polysaccharides are example for biopolymer systems (Sundar et al., 2010). Protein based nanoparticles are commonly used for drug delivery due to their ease of particle size control, biodegradability, stability, possibility for modifying its surface. Also, problems related to toxicity issues, such as immunogenicity observed less compared to other nanoparticle materials (Hong et al., 2020). Protein based nanoparticles can be synthesized from different kind of proteins found in bloodstream such as ferritin, hemoglobin and albumin (Figure 1.2) (Iqbal et al., 2021).

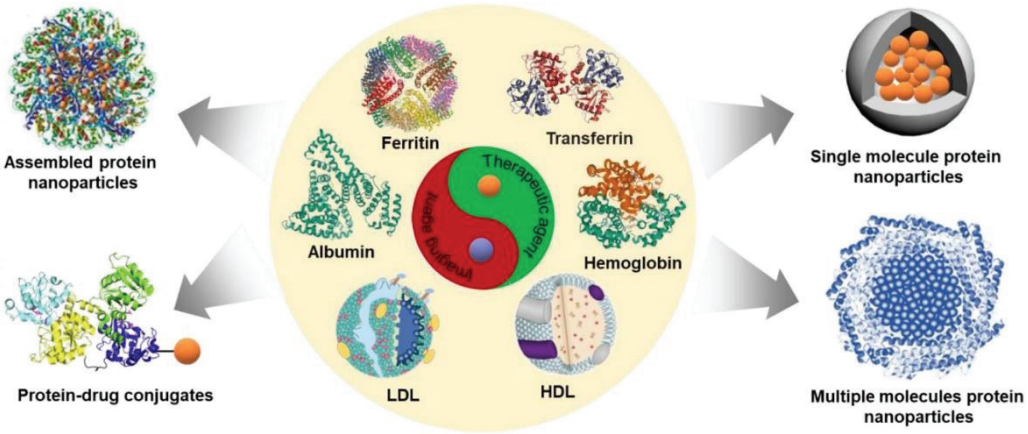

Figure 1.2. Protein based nanoparticles (Iqbal et al., 2021).

The plasma protein albumin which is one of the most abundant proteins draws attention for the preparation of nanocarrier systems. Its binding capacity is high, it can bind with both hydrophobic and hydrophilic drugs. Albumin has virtually minimal toxicity, immunogenicity and relatively long half-life. Also, it is able to specifically target inflammation sites (Spada et al., 2021). It is a globular protein responsible for maintaining the osmotic pressure, binding and transporting compounds such as drugs, hormones, enzymes, fatty acids and vitamins in blood circulation (Amighi and Djomeh, 2020). It is also soluble in water and diluted salt solution, stable at different pH values (in the range of 4–9) and at high temperatures (60 ^{0}C up to 10 h) (Sombat et al., 2020). Albumin can be obtained from different sources such as egg white (ovalbumin), bovine serum albumin

(BSA) and human serum albumin (HSA) (Verma et al., 2018). Structurally, albumin has 3 homologous domains named as I, II and III. Each of these domains has two sub-domains, A and B. These sub-domains provide required binding sites for ligand binding. Domain IIA and IIIA are also named as Sudlow I and Sudlow II, respectively (Mondal et al., 2017). Through these sites, albumin can bind or interact with different molecules and ligands (Figure 1.3) (Ghuman et al., 2005; Sand et al., 2015; Tatlidil, 2015). Thus, albumin is one of the nanocarrier material for drug loading and delivery.

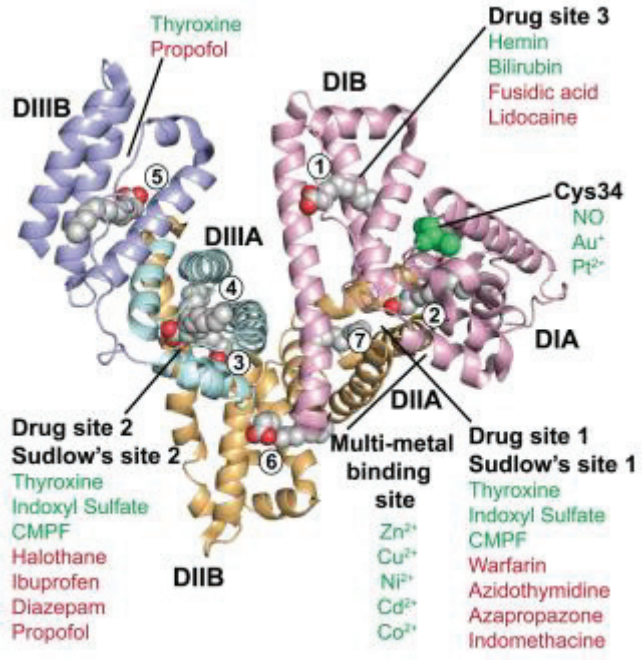

Figure 1.3. Structure and binding sites of HSA (Sand et al., 2015).

In the literature, BSA is studied more frequent compared to HSA due to its easier production and reasonable price. The primary structure of BSA is 76% similar to the HSA. Also, crystal structures and the ligand binding properties of both proteins are similar (Sugio et al., 1999; Majorek et al., 2012; Akdogan et al., 2012).

Aspartic acid and glutamic acid provide negative charge to the protein surface with their carboxyl groups. There are 99 carboxyl groups in a BSA protein. Lysine and arginine provide positive charge to the protein surface with their amino groups. There are 59 amino groups in a BSA protein. 30-35 of amino groups in BSA are located in an area suitable for functionalization (Hermanson, 2013). Isoelectric point of albumin is in the pH range of 4.8 – 5.6, has a negative charge in the physiological environment (Barbosa et al., 2010). The properties of albumin can be changed and improved by

functionalizations of these active surface groups. In the literature, BSA has been modified and studied by binding molecules such as amine-containing molecules, citric acid, dopamine, carboxymethyl and acetyl (Zhu et al., 2017; Vismara et al., 2017; Akdogan et al., 2016; Fukuzawa et al., 2005).

1.3. Stimuli Responsive Nanocarriers

Stimuli responsive nanocarriers are the systems that drug releasing mechanism is based on a trigger such as exogenous and endogenous stimulus (Chen et al., 2016). Sensitivity of nanocarrier to a specific stimuli provides more controllable drug release profiles and improved stability for drug delivery. Stimuli of the nanocarrier can be tailored due to the microenvironment of the target cells (Mura et al., 2013).

Exogenous stimuli are manually controlled by external stimulus such as light, heat, magnetic fields, and ultrasound (Jia et al., 2021). Using of these materials require application of the stimuli to a specific location or organ to trigger releasing of the ligand (Majumder and Minko, 2021).

Endogenous stimuli-sensitive nanocarriers are sensitive to several endogenous stimuli factors such as pH, redox potential and enzymes (Majumder and Minko, 2021). Redox-sensitive nanomaterials contain disulfide linkage which can be rapidly cleaved by reductive substance glutathione (GSH) via thiol-disulfide exchange. It is possible in environment with high concentration of GSH which can be provided by in the intracellular environment of tumor cells (approximately 2–10 mM). This system remains relatively stable in the extracellular environment which has a lower concentration of GSH (approximately 2–20 μM) (Sun et al., 2021). For enzyme-responsive nanocarriers, change in the expression of specific enzymes, including proteases, phosphatases, and glycosidases can be detected in tumor or inflammatory areas. When nanocarriers are sensitive to these changes, delivery of drugs at the desired biological location becomes possible (Li et al., 2020). For the pH-sensitive nanocarriers, pH of the environment changes physical property of nanocarrier including solubility, conformation such as hydrophilic/hydrophobic balance and configuration such as crystalline/amorphous transition (Karimi et al., 2016). These alterations can be reversible or irreversible. Chain or bond conformation may provide reversible systems. Otherwise, dissolution/swelling

of polymers by pH variation causes collapse or degradation of the carrier so polymer has irreversible pH responsive system.

At extracellular areas where cancerous tissues are found, pH is in the range of 6.4 – 6.8, which is more acidic compared to healthy tissues, pH 7.4 (Van Sluis et al., 1999; Choi et al., 2013; Calcinotto et al., 2012). This difference occurs due to the production of higher amount of lactic acid from cancer tissues (Zhao et al., 2017; Gao et al., 2022). In addition, the pH values of intracellular endosomes and lysosomes have lower pH valuesthan blood, pH 7.4. At these areas, pH decreases to 6.5 in endosomes and below 5.0 in lysosomes (Yoshida et al., 2013; Such et al., 2015). By taking advantage of these pH variety in human body, drug loaded pH responsive nanocarriers can be rapidly degraded and drug release in these organelles. For pH-responsive nanocarrier, Chen et al. developed a multi-functionalized nanosized albumin-based drug-delivery system with tumor targeting, cell-penetrating and pH-responsive properties. Tumor targeting ligand cRGD was conjugated with BSA and formed cRGD-BSA which was negatively charged. Then, cRGD-BSA and positively charged cell-penetrating peptide (CCP) KALA self-assembled into dual-functionalized albumin nanoparticle. Lower pH in the tumor cell which is close to the isoelectric point of BSA (pI = 4.7) and surface charge of the albumin decreased, significantly. It can be attributed to decrease electrostatic interaction between BSA and KALA which caused to the disassembly of nanoparticles (Chen et al., 2015). Li et al. designed a novel nanophotosensitizer by one-step covalent assembly of dopamine and genipin to obtain pH sensitive drug carrier via catechol–boronate bonding. Catechol–boronate bonds are stable under a neutral or alkaline pH values. However, it can easily dissociate in the environment with lower pH. In the study, the anticancer drug bortezomib (Btz) was loaded to monitor drug release which was carried out at pH 7.4 and 5.4 to imitate the physiological pH in normal tissues and intracellular endosomes, respectively. At pH 7.4, burst release occurred in the first 2 h and totally 38% of Btz was released at 12 h time period. On the other hand, at pH 5.4, rapid drug release in the first 2 h occurred, and then Btz release continued over the following period of time and reached nearly 94% of Btz releasing (Li et al., 2019).

1.4. Mussel Inspired pH Responsive Polymers

Marine mussels are known with the ability to stick various surfaces in seawater such as ship hulls, oil platforms, and pipelines to meet their basic vital needs (Silverman and Roberto, 2007). It is possible with high 3,4-dihydroxy-L-phenylalanine (DOPA) amino acid content (up to 27% mole) of mussel foot proteins (Mfps) which have adhesive properties found in their byssal plaque (Figure 1.4(A)) (Heidarian et al., 2020). In Figure 1.4(B) synthesis of DOPA by post-translational modification of tyrosine (Tyr) by tyrosinase enzyme is shown (Bilotto et al., 2019).

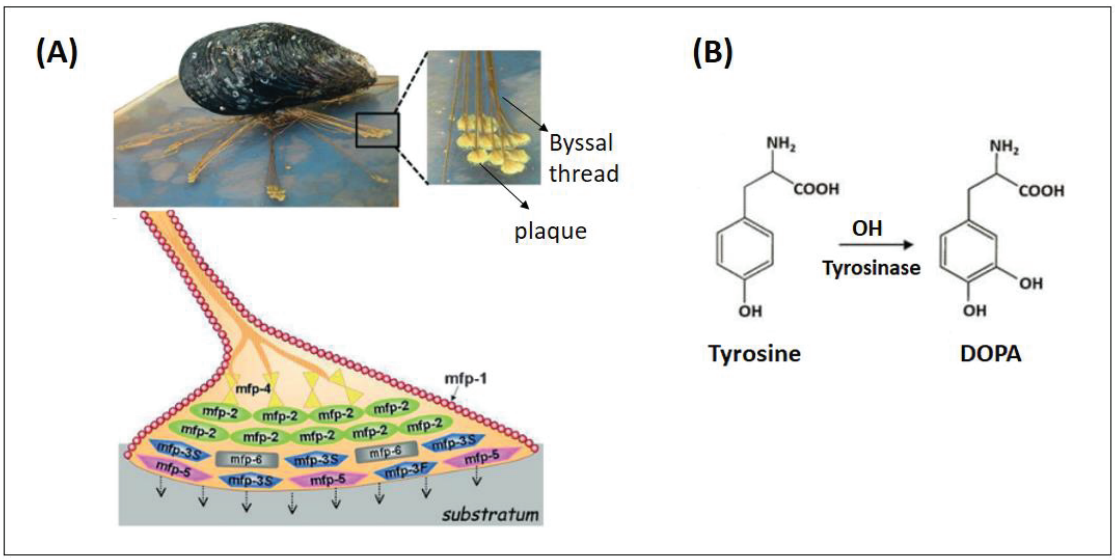

Figure 1.4. (A) Mussel threads and the proteins (mussel foot proteins, Mfps) that provide adhesion in the plaques at the end of the thread (Akdogan et al., 2014), (B) Synthesis of DOPA from the tyrosine amino acid by tyrosinase enzyme.

DOPA can strongly adhere to many hydrophilic and hydrophobic surfaces, such as teflon, mica, TiO_2, gold, polystyrene, etc. (Wei et al., 2013; Dalsin et al., 2005; Lu et al., 2013; Kırpat et al., 2017; Goksel and Akdogan, 2019; Yildiz et al., 2020). In these studies, the adhesive property of DOPA is explained by the hydroxyl groups in the catechol group (Figure 1.5). These groups can make hydrogen bonds with hydrophilic surfaces and form bidentate metal-oxygen bonds with metals. They can also interact with aromatic and hydrophobic surfaces and ligands with hydrophobic surfaces.

Dopamine is one of the catechol derivatives commonly used as coating material or conjugation with polymers for medical applications due to its water solubility (Song et

al., 2021; Fan et al., 2016; Ma et al., 2014). Dopamine can be conjugated to polymers by polymers' functional groups such as – NH_2, – COOH and – OH through amide, urethane and ester linkages (Kord Forooshani and Lee, 2017). The important part of preparing catechol-functionalized polymers is protecting the catechol side chains against oxidation and undesired chemical reactions (Kord Forooshani and Lee, 2017). For catechol-metal coordination bonds, oxidation of catechol side chains causes losing pH sensitivity and reversibility of the bonds. Oxidation of catechol groups is caused by alkaline conditions and presence of oxidation agents (Göksel and Akdogan, 2019). Mechanism of catechol oxidation is shown in Figure 1.5.

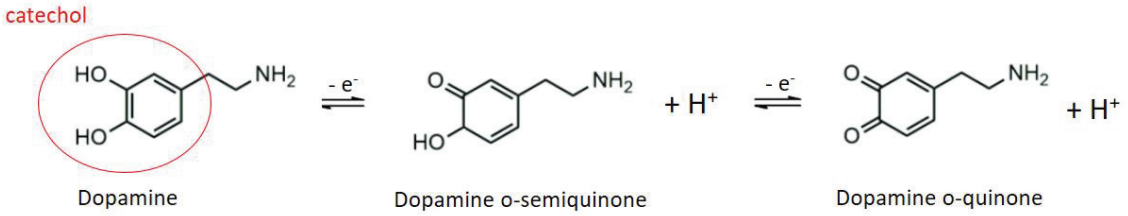

Figure 1.5. Oxidation of non-oxidized dopamine to dopamine o-semiquinone and dopamine o-quinone.

In the literature, the most interests are on the metal–catechol coordination bonds due to their pH sensitive nature. These different forms of coordination bonds are named as mono-, bis- and tris- due to their stoichiometry (Figure 1.6). With increasing pH of the environment, strength of the coordination bond increases in a broad range (approximately between 25% and 95% of a covalent bond) (Li and Zuo, 2020).

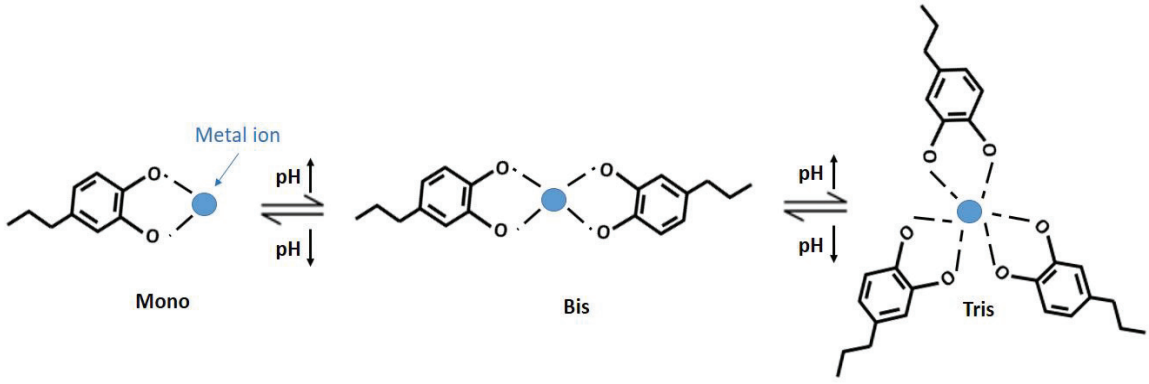

Figure 1.6. Metal–catechol coordination polymer networks depend on pH.

In literature, catechol-metal coordination bonds are used for different areas such as thermosets (He et al., 2020; Shen et al., 2023), material strengthening (Cheng et al., 2019) and biomedical applications (Qiao et al., 2014; Andersen et al., 2017; Ejima et al., 2018; Hebel et al., 2022).

Lu et al. fabricated hydrogels from four-armed poly(ethylene glycol) modified with dopamine end groups with Fe(III) ions. By changing pH, mono-, bis- and tris-catechol–Fe(III) coordination can be reversibly changed (Figure 1.6). Coordination bond fixed the temporary shape, then recovered the original shape. Also, bonds played an important role for the enhancement of the mechanical properties of the hydrogel (Lu et al., 2019). Hebel et al. prepared catechol-Fe(III) coordination mediated human serum albumin nanoparticles (HSA NPs) and hydrogels. They showed that more concentrated solution resulted albumin hydrogel formation while diluted protein solution formed albumin nanoparticles. Depending on the catechol:Fe(III) ratio and the pH, HSA NPs between the sizes of 19 to 27 nm were obtained. For hydrogels, macroscopic hydrogel matrixes with varying mechanical strength from G', G'' = 0 Pa to G' = 4.4 kPa, G'' = 0.6 kPa were obtained by adjustment of pH and the amount of Fe (III) (Hebel et al., 2022).

For catechol-metal coordination bonds, different metals such as iron(III), copper(II), cobalt(II), zinc(II), nickel(II), titanium(IV), aluminum(III), vanadium(III), manganese(III) were used (Filippidi et al., 2017; Jia et al., 2019; Ayad et al., 2016; Xu et al., 2013; Sever and Wilker, 2004). Due to the metal used for catechol-metal coordination, required pH for reaching its mono- bis- or tris- form can vary. Holten-Andersen et al. synthesized hydrogel with catechol-modified PEG polymer (cPEG) and different metal salts; VCl_3, $FeCl_3$, or $AlCl_3$. At pH 8, UV-Vis absorption of catechol-V(III) and catechol-Fe(III) samples showed typical of tris-catechol–V(III) and bis-catechol–Fe(III) coordinations while catechol-Al(III) sample showed the weakest absorbance. In the low energy region of Raman spectrum, catechol–V(III) coordinate polymer networks at pH 8 have a strong and well-defined charge transfer (CT) band suggests tris-complexation while catechol–Fe(III) coordinate polymer networks is weaker, corresponds bis-complexation at the same pH. Catechol-Fe(III) complex showed similar CT band at pH 12.0. These results show that catechol-V(III) complex achieves tris complex at lower pH compared to catechol-Fe complex (Holten-Andersen et al., 2014).

1.5. Albumin Nanoparticles Preparation Methods

There are three common methods for preparing albumin nanoparticles; chemical methods (emulsion and complex coacervation), physical methods (electrospray and nano spray drying), and self-assembly methods (desolvation and self-assembly) (Figure 1.7) (Hong et al., 2020).

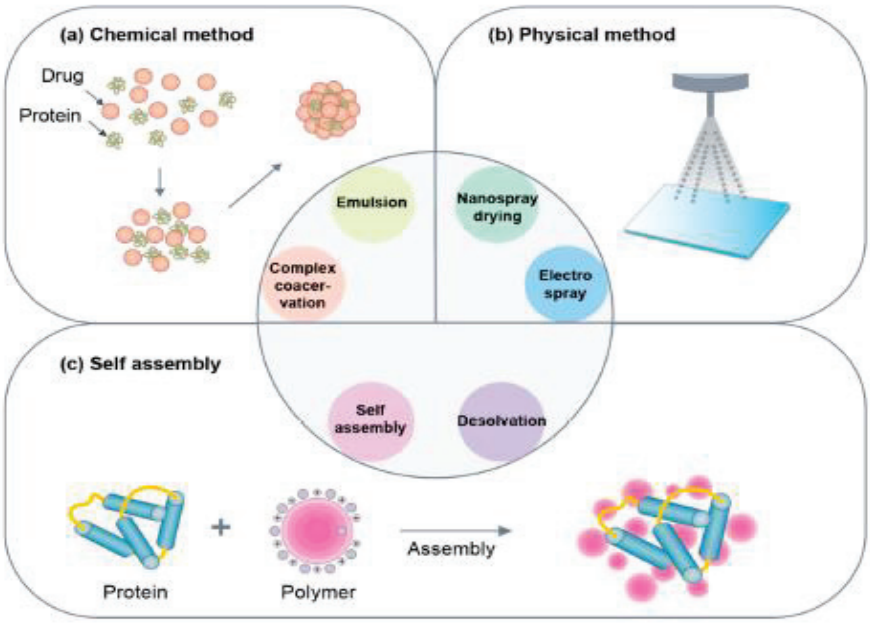

Figure 1.7. Categorization of methods for preparing protein nanoparticles: (**a**)chemical method, (**b**) physical method and **(c**)self-assembly method (Hong et al., 2020).

Chemical techniques include chemical reactions based on the process a product precipitates from a liquid (or solution) phase containing a precursor. Soluble species become insoluble to enable to precipitate (Hachem et al., 2022). By chemical techniques, highly stable, size-controlled nanoparticles can be obtained. However, surfactant and stabilizer requirement for emulsification method and scale-up difficulty for complex coacervation method are main drawbacks for chemical nanoparticle synthesis methods (Hong et al., 2020, Demirkurt et al., 2018).

Physical techniques include spray-drying methods which is the process of transition the material from liquid to powder. In typical spray-drying steps, materials are atomized and dried through gas. Particles were formed and collected. Advantages of

spray-drying are simplicity of production process, fast drying and well dispersion of products. However, the traditional spray-drying device has difficulty to capture particles size with less than 2 μm. Also, hot air-drying process causes denaturation and inactivation of albumin. As a result, physical methods are not suitable for producing albumin nanoparticles (Meng et al., 2022).

In the self-assembly methods, covalent conjugations are aimed to improve the hydrophobicity of proteins to obtain to self-assemble into nanoparticles (Ding et al., 2014). Hydrophobicity of protein can be increased by reducing the internal disulfide bond of albumin which is named as self-assembly method. Common reducing agents are β-mercaptoethanol, dithiothreitol, and cysteine (Meng et al., 2022). In desolvation method, organic solvent is added for changing the protein structure and causes reducing solubility of the protein. Then, precipitated nanoparticles are bridged by a crosslinker (Hong et al., 2020; Sozer and Akdogan, 2022). Since self-assembly method requires chemical modification to increase self-assembly force, desolvation draws attention for albumin nanoparticle synthesis due to simplicity of preparation, rapid reaction, repeatability and no requirement for surfactant (Meng et al., 2022).

Desolvation procedure includes continuous or intermittent dropwise addition of a desolvating agent such as methanol, acetone, or ethanol into an aqueous solution of albumin under constant stirring. Turbidity observation during desolvating agent addition indicating that nanoparticles are formed (Langer et al., 2003). In this stage, formed nanoparticles are not stable and they may aggregate. Crosslinker is added to stabilize nanoparticles such as glutaraldehyde or N-(3-dimethylaminopropyl)-Nethylcarbodiimide (EDC). In glutaraldehyde usage, nanoparticles are strengthened by condensation cross-linking of the amino moieties in the albumin side chain. When EDC used as a crosslinker, an amide bond is formed between the amino and carboxyl side groups of amino acids (Srivastava and Prajapati, 2020). Schematic of albumin nanoparticle preparation with desolvation method is given in Figure 1.8 (Karami et al., 2020).

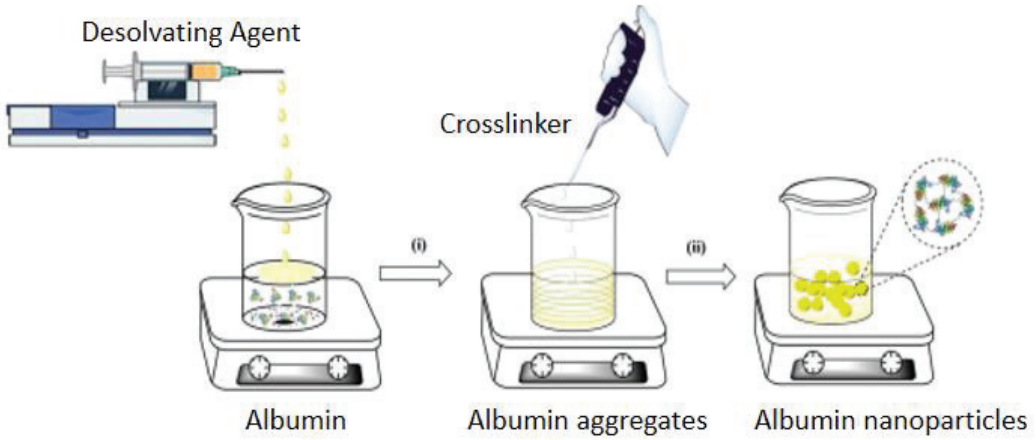

Figure 1.8. Preparation of albumin nanoparticles with desolvation method (Adopted from Karami et al., 2020).

In recent years, albumin nanoparticles synthesized by the desolvation method have been studied frequently in antitumor applications. Ziaaddini et al. studied BSA nanoparticles prepared by desolvation techniques for improved efficacy and reduced cytotoxicity for an anticancer drug (Ziaaddini et al., 2020). Lee et al. optimized parameters for desolvation technique such as the speed of ethanol addition, pH of protein solution and concentration of HSA were optimized to produce HSA nanoparticles with sizes ranging from 100 to 300 nm (Lee et al., 2016). It has been found that particle size of albumin nanoparticles depends on the protein concentration, volume, pH, and temperature of the desolvating agents.

1.6. Doxorubicin and Its Interaction with Albumin

Doxorubicin (DOX) is generally used as an anthracycline antibiotic in the treatment of breast cancer, acute leukemia, Hodgkin and non-Hodgkin lymphomas and lung cancer (Singal and Iliskovic, 1998). Doxorubicin binds to DNA by intercalation to prevent its biosynthesis and stop the proliferation of cancerous cells (Agudelo et al., 2014). However, dose-dependent toxicity of the drug in the body, emergence of drug resistance, side effects such as hair loss, vomiting, rash and heart failure (cardiotoxic) limit the use of doxorubicin in treatment (Singal and Iliskovic 1998; Chatterjee et al., 2010). Chemical structure of DOX is given in Figure 1.9.

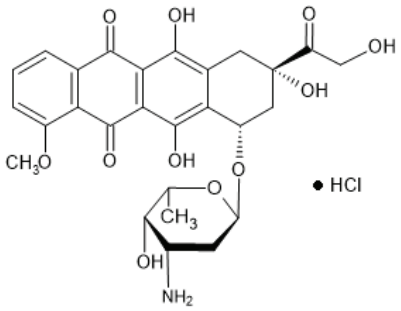

Figure 1.9. Structure of doxorubicin.

In the literature, different materials for doxorubicin delivery such as poly(butyl cyanoacrylate) (Gulyaev et al., 1999), poly(isohexylcyanoacrylate) (Cuvier et al., 1992), poly(lactic acid-co-glycolic acid) (Park et al., 2009), chitosan (Janes et al., 2001), gelatin (Leo et al., 1999), liposome (Lukyanov et al., 2004) and serum albumin (Dreis et al., 2007; Yang et al., 2018) were used. Albumin nanocarriers are commonly used for DOX delivery (Parajapati et al., 2021; Aziz et al., 2022; Honary et al., 2010; Onafuye et al., 2019; Cakan-Akdogan, 2022). Shalbafan et al., studied interaction between HSA and DOX by docking technique. Docking study showed that doxorubicin is able to interact with HSA with one arginine residue by hydrogen bond, in fact the hydroxyl group is inserted in a hydrophobic pocket. Gibbs free energy ($\Delta G°$) is equal to -9.1 kcal/mol which shows that it is a spontaneous process ($\Delta G° < 0$). The association constant value ($K_a \approx 8\times10^3$ L.mol^{-1}) shows its efficient bio-distribution by blood plasma (Shalbafan et al., 2019).

Yang et al. showed that DOX release rate from BSA NPs is faster at pH 5.0 compared to that of at pH 7.4 due to the breaking of the Schiff base bond in acidic conditions. The cumulative release amounts of DOX for 24 hours were found to be 30, 55 and 70% at pH 7.4, 6.5 and 5.0, respectively (Yang et al., 2020). Chaiwaree et al. fabricated human serum albumin submicron particles (HSA-MPs) by using the Co-precipitation–Crosslinking–Dissolution technique (CCD technique). Then, DOX was loaded into the submicron particles by absorption method. Entrapment efficiency of DOX was 25% of the initial amount. In vitro release performed in PBS buffer at pH 7.4 was less than 1% within 5 h. In vitro cytotoxicity and cellular uptake of DOX-HSA-MPs were evaluated by using lung carcinoma cell line A549 and albumin submicron particles reduced the cell metabolic activities after 72 h (Chaiwaree et al., 2020). Kimura et al.

prepared DOX loaded HSA NPs by desolvation method to investigate anti-tumor effects and bio-distribution in vitro and in vivo. 2D and 3D colon 26 cell cultures were used to evaluate the cytotoxicity of NPs. Furthermore, the bio-distribution and the anti-tumor activity of NPs in colon 26-bearing mice were investigated. DOX loaded HSA NPs showed cytotoxicity in colon 26 cancer cell cultures, while the cytotoxicity was higher in free DOX. Compared to free DOX, in vivo antitumor activity was higher with the NPs, although their accumulation in tumors was much the same. These results show that factors other than accumulation contribute to the enhanced antitumor activity of these NPs. Furthermore, DOX loaded HSA NPs resulted in suppression of metastasis (Kimura et al., 2019). Kim et al. used recombinant mussel foot proteins (Mfp-1) to form DOX-loaded NPs with the help of Fe(III). Drug release after 8 hours was found to be around 80% in the pH 6.0 medium where mono- and bis- coordination are present. Yet, the cumulative release was found to be 50% at pH 7.4 where only bis- coordination is present (Kim et al., 2015)

1.7. Aim of the Thesis

In this study, controllable drug release was obtained by synthesizing pH-sensitive nanoparticles via formation of catechol-metal coordination bonds. At different pH values, catechol-metal coordination bonds have different stoichiometry (e.g. mono-, bis- or tris-) which change the strength of the bond, dramatically. Albumin nanoparticles are commonly used as carrier systems due to their non-toxicity, biodegradability and stability over long periods of storage. Variability of functional groups on serum albumin provides ability of surface modification so, different ligands or polymers can bind to their surface. BSA protein was conjugated with catechol containing dopamines (D), so it is possible to form pH responsive coordination bonds with metal ions during NPs synthesis.

D-BSA NPs were synthesized by desolvation method followed by vanadium-based crosslinking. Catechol-containing dopamine molecule and V(III) ions can form structures in different coordination which are sensitive to pH. While they can form mono-structure bonds at acidic pH, they can form chelate bonds as bis- and tris- at higher pH values. Thus, the stability of nanoparticles will depend on the catechol-V(III) coordination bonds. Since pH of tumor tissues is lower than pH of blood, decrease of the pH of the medium (< 7.4), the catechol-V(III) coordination became mono-bis-dominated,

which will lead to the drug releasing. Doxorubicin, a chemotropic drug, was used as a model drug to demonstrate that the drug releasing of D-BSA NPs. In this way, it was aimed that the doxorubicin drug remains in the D-BSA NPs in blood circulation in a controlled manner and rapidly released in relatively more acidic tumor tissues.

CHAPTER 2

EXPERIMENTAL

2.1. Materials

Bovine serum albumin (BSA, MW: 66.5 kDa lyophilized powder, >96%), N-(3-Dimethylaminopropyl)-N′-ethylcarbodiimidehydrochloride (EDC), N-Hydroxysuccinimide (NHS), dopamine hydrochloride, vanadium (III) chloride, phosphate-buffered saline (PBS), albumin-fluorescein isothiocyanate conjugate (FITC), 16-doxyl stearic acid (16-DSA), 4-hydroxy-2,2,6,6-tetramethylpiperidine-1-oxyl (TEMPOL), KOH, acetone, methanol, ethanol, propanol were purchased from Sigma – Aldrich. Acetonitrile was purchased from Merck. Doxorubicin hydrochloride was purchased from SelleckChem. All chemicals and solvents were analytical grade and utilized without any purification procedures. The pH of the solutions was adjusted with hydrochloric acid and sodium hydroxide.

2.2. Preparation of dopamine conjugated BSA (D-BSA) protein

Dopamine hydrochloride (72 mg) was dissolved in 3 mL PBS (0.02 M, pH 7.2) and then was added into BSA solution (72 mg in 3 mL deionized water). They were stirred under argon gas for 15 min at 37 ^{0}C. The pH of the mixture was adjusted to 6.0 by adding HCl (1 M), intermittently. Subsequently, EDC (72 mg) and NHS (72 mg) were added into the mixture and kept at 37 ^{0}C for 2 h under argon gas. (Figure 2.1) The reaction was stopped by the addition of 4 M acetate buffer (4 M, pH 6). D-BSA was purified by ultra-pure water to eliminate unreacted amount of EDC, NHS and dopamine hydrochloride by 5 cycles of centrifugation by using centrifugal filter (molecular cut off: 50 kDa) (12,000 rpm, 2 min). After washing procedure, the D-BSA protein was collected from centrifugal filter and lyophilized. It was stored at 4 ^{0}C. The yield of the product was about 75%.

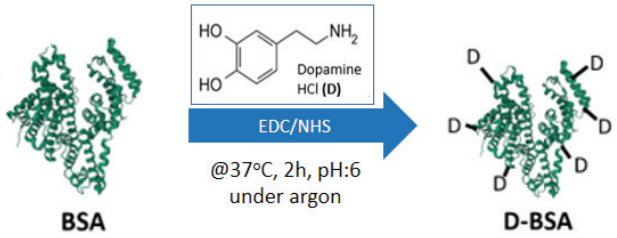

Figure 2.1. Modification of BSA protein with dopamine molecules.

2.3. Preparation of D-BSA NPs

Lyophilized D-BSA protein (9.5 mg) was dissolved in 980 µL of pure water and stirred for 15 minutes at 750 rpm. Then, pH of the solution was increased to 7.4 by addition of 20 µL NaOH (0.1 M), intermittently. Afterwards, 5 mL of acetone:water (4:1)(v/v) was added dropwise to the aqueous solution of D-BSA at a rate of 1 mL/min with a syringe pump and 36 µL of VCl_3 solution (0.081 M) was added to nanoparticle suspension at 1200 rpm. After the addition of VCl_3, pH of the nanoparticle suspension was increased to 8 by intermittent addition of NaOH (0.5 M) in each 4 min. and stirred for overnight. Effect of vanadium addition is shown in Figure 2.2. Next, obtained D-BSA nanoparticles were placed in eppendorf tubes for centrifuge. Unbound D-BSA, excess solvents and VCl_3 solution were discharged by centrifuging the nanoparticles at 12,000 rpm for 15 minutes. After each centrifuge, supernatants were removed from the eppendorf tubes and remain pellets were washed with 1 time by methanol:water (1:1)(v/v) and 2 times by methanol:water (1:3)(v/v) for the purification of the nanoparticles. pH of methanol & water mixtures was kept at 8. The yield of the product was about 65%.

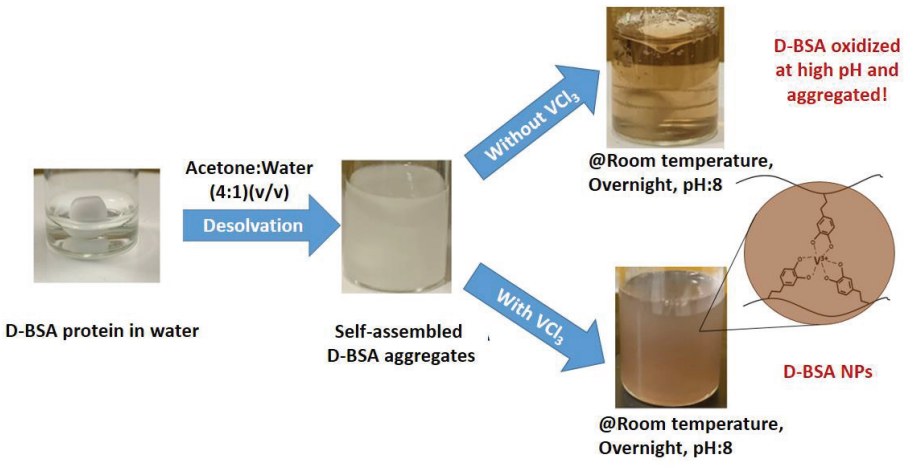

Figure 2.2. D-BSA nanoparticle formation.

2.4. Characterization of BSA, D-BSA proteins and D-BSA NPs

Zeta potential of the modified and native proteins were analyzed by Malvern Dynamic Light Scattering (DLS) Nano-ZS instrument (Worcestershire, UK). Molecular mass of D-BSA and BSA were determined by mass spectrometer Bruker Autoflex-III (smartbeam) MALDI TOF/TOF system. Catechol groups on modified BSA was determined by LAMBDA 365 UV–visible spectrophotometer (PerkinElmer). Dried protein samples were analyzed by Attenuated Total Reflectance Fourier Transform Infrared (ATR-FTIR) spectrometer (Thermo Scientific Nicolet iS50). Fluorescence analysis was performed by FL 8500 Fluorescence Spectrophotometer (PerkinElmer). Conformational and antioxidant studies of BSA and D-BSA proteins were performed with a CMS 8400 (Adani) benchtop X-band electron paramagnetic resonance (EPR) spectrometer at room temperature. 26 mM 16-doxyl stearic acid (16-DSA) was prepared in 0.1 M KOH and mixed with different concentrations of BSA or D-BSA to get the final 16-DSA concentration of 1.5 mM. Protein:16-DSA molar ratios were set to 1:2, 1:4 and 1:7. Antioxidant studies were carried out using 1.4 mM TEMPOL prepared in 0.01 M PBS buffer at pH 7.4. TEMPOL solution was mixed with 1.4 mM BSA or D-BSA protein solution prepared in the same PBS solution with 1:1 (vol/vol) ratio, and the mixture of TEMPOL and proteins were measured with EPR spectrometer immediately and after 24 hours.

For D-BSA NPs characterization, purified NPs were dissolved in ultra-pure water at pH 8.0. SEM analyses were used for examining the size, shape and distribution of the nanoparticles (SEM, FEI QUANTA 250 FEG). Dissolved NPs were diluted 3 times with ultra-pure water. 4.5 μL solutions of NPs were dropped onto aluminum foil. At the next day, the dried samples were coated with gold in a vacuum using an EMITECH K550X for SEM imaging. The accelerating voltages ranged between 5 and 7 kV. In addition, the size and PDI values of NPs were measured by using a Malvern dynamic light scattering (DLS) at a wavelength of 632 nm. The scattering angle was set at 173º and, Malvern dynamic light scattering (DLS) Nano-ZS instrument (Worcestershire, UK) was used to calculate the zeta potentials of NPs. For the size and zeta potential measurements, dissolved NPs were diluted 10 times with ultra-pure water.

2.5. Loading of DOX to D-BSA Nanoparticles

For DOX loading, incubation method was used. D-BSA nanoparticles (3.1 mg) was dissolved in PBS (0.005 M, pH 7.4). 15.5 µL of DOX-HCl (43 mM) was added drop by drop on nanoparticle and they were stirred for overnight, 300 rpm in the dark.

For the determination of unbound DOX, 15.5 µL of DOX-HCl (43 mM) was added drop by drop on PBS (0.005 M, pH 7.4) without D-BSA nanoparticle with same reaction conditions of incubation. The next day, DOX incubated D-BSA nanoparticles and DOX in PBS were transported to eppendorf tubes in order to be centrifuged at 12,000 rpm for 15 minutes. UV of supernatant of nanoparticle and DOX in PBS was measured by using LAMBDA 365 UV–visible spectrophotometer (PerkinElmer). For the calibration curve, DOX stock solutions in PBS (0.005 M, pH:7.4) were prepared. The curve was linear and passed through the origin ($R^2 = 0.9988$, n = 5). Entrapment efficiency and drug loading were determined by formula 2.1 and formula 2.2, respectively.

$$Entrapment\ Efficiency\ (\%) = \frac{Initial\ drug\ weight - Drug\ weight\ in\ supernatant}{Initial\ drug\ weight}\ x\ 100\ (\%) \qquad (2.1)$$

$$Drug\ Loading\ (\%) = \frac{Weight\ of\ drug\ in\ nanoparticles}{Total\ weight\ of\ nanoparticles}\ x\ 100(\%) \qquad (2.2)$$

2.6. In Vitro Release Studies of DOX from D-BSA NPs

In vitro release of DOX from D-BSA NPs prepared with DOX:D-BSA NPs molar ratios 15:1 were performed in 0.01 M PBS buffer at pH 7.4, 5.5 and 4.2. D-BSA NPs-DOX (1.93 mg) were dispersed in 800 µL of 0.01 M PBS buffer. Then, the solutions were placed into the 800 µL D-tube dialyzers (Merck, MWCO 3.5 kDa). The dialyzer tube was placed in a beaker at 37 ºC containing 32 mL of PBS buffer at pH 7.4, 5.5 or 4.2 under 500 rpm stirring. At predetermined time points, 2 mL of sample was collected and measured by UV–visible spectrophotometer to monitor the released amount of DOX from D-BSA NPs. After UV-Vis measurements, the 2 mL of samples were put back in the beakers. Schematic of DOX release from D-BSA NPs is given in Figure 2.3.

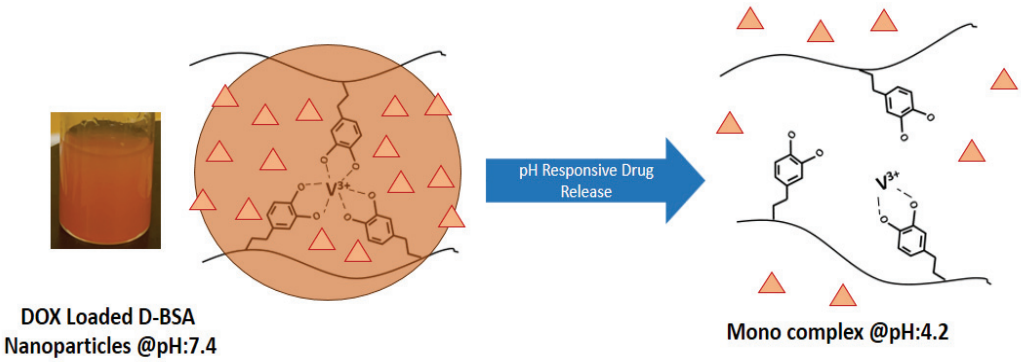

Figure 2.3. Schematic of DOX release from D-BSA NPs.

2.7. Cell Uptake Assay

MCF-7 breast cancer cells were cultured in Dulbecco's Modified Eagle Medium (DMEM) with 10% Fetal Bovine Serum (FBS), 1% penicillin and 1% streptomycin. FITC-labeled D-BSA NPs and DOX-loaded FITC-labeled D-BSA NPs were suspended in DMEM and used for cell uptake assay as described previously (Akdogan et al., 2022). Cells stained with Dil (Thermo Scientific) were seeded at 50000 cells/well density on 8 well imaging slides. Attached cells were treated with 0.075 mg/mL FITC-labeled D-BSA NPs or 0.075 mg/mL DOX-loaded FITC-labeled D-BSA NPs for 24 hours. Excess NPs were removed by washing with 1X PBS-T, and cells were fixed with 4% PFA, and post stained with DAPI as described previously (Akdogan et al., 2022). Images were acquired with Zeiss LSM880 confocal microscope, with 40X/W objective, Z-stacks with 7 µm interval were captured. Background subtraction and maximum Z-projection was applied with ImageJ software.

2.8. Cell Viability Assay

MCF-7 cells were seeded 7,500 cells/well in 96-well plates, treated with D-BSA NPs (or DOX-loaded D-BSA NPs) at final concentrations of 0.2 mg/mL, 0.1 mg/mL, 0.05 mg/mL, 0.025 mg/mL, 0.0125 mg/mL, 0.0025 mg/mL and 0.0005 mg/mL or free DOX at final concentrations of 36 µM, 18 µM, 9 µM, 4.5 µM, 2.25 µM, 0.45 µM, 0.09 µM. After 24 hours, incubation with the NPs or DOX, MTT cell viability assay was performed as described previously (Cakan-Akdogan et al., 2022). For quantification of formazan,

absorbance at 570 nm was measured with Thermo Fisher Multiskan Go. The decrease in signal was used to calculate cell survival compared to control wells with 100% survival. Each measurement was done in 4 replicas, and % viability was calculated.

CHAPTER 3

RESULTS AND DISCUSSION

The main purpose of this study was to produce pH responsive nanoparticles as a nanocarrier system for transportation of drugs in the body. First, albumin was functionalized by using catechol-containing dopamine hydrochloride (D). Synthesized D-BSA was analyzed to determine dopamine molecules conjugated on BSA. Then, D-BSA proteins were desolvated to obtain D-BSA NPs upon addition of V(III) ions. Tris-coordination bonds with catechol groups of dopamine on BSA surface and V(III) ions produced D-BSA nanoparticles. DOX was loaded as a model drug and drug loaded nanoparticles were characterized by using different methods. Releasing of DOX was studied at different pH conditions and effect of pH on NPs was shown.

3.1. Characterization of BSA and D-BSA Proteins

3.1.1. MALDI-TOF Mass Spectrometry Analyses of BSA and D-BSA

Here, we functionalized BSA proteins with catechol-containing dopamine (D) molecules to obtain dopamine conjugated BSA (D-BSA) in the presence of coupling agent of EDC. MALDI TOF mass spectrum shows that the molecular weight of BSA increases from 66643 g/mol to 68657 g/mol upon conjugation of average 15 dopamines to BSA (Figure 3.1). This number of bound dopamines was obtained by reacting the excess dopamine with the available carboxylic acid side chains of 99 amino acids (Asp and Glu) found in BSA. The weight ratio of dopamine in D-BSA was found to be 3.3%.

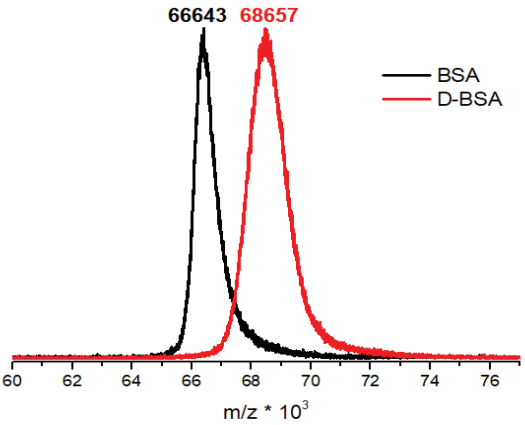

Figure 3.1. MALDI-TOF mass spectra of native BSA (black) and dopamine conjugated BSA (D-BSA) (red) proteins.

3.1.2. Zeta Potential

Dopamine conjugated BSA (D-BSA) was prepared through an amide coupling between the BSA and dopamine. Amine group of dopamine was conjugated with carboxylic acid side groups of amino acids e.g. aspartic acids (Asp) and glutamic acids (Glu) in BSA. Upon dopamine conjugation, the negative net charge of BSA decreased from -11 mV to -8 mV at pH 7.0. (Figure 3.2). In order to compare isoelectric points of native BSA and D-BSA, zeta potentials of BSA and D-BSA at different pH levels (3.0 - 9.0) were studied. As the pH of BSA was increased from 3.0 to 5.0, the zeta potential decreased from +20 to 0. As the pH of D-BSA was increased from 3.0 to 5.5, the zeta potential decreased from +10 to 0. The high zeta potential of the protein surface shows that the its surface has polar properties.

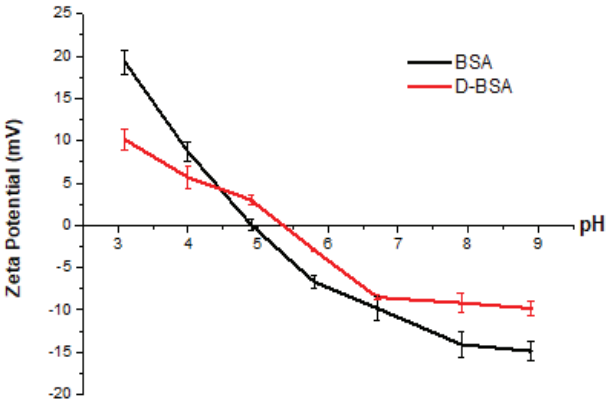

Figure 3.2. The zeta potentials of BSA (black) and dopamine conjugated BSA (D-BSA) (red) proteins at pH values ranging from 3.0 to 9.0 in water.

3.1.3. ATR-FTIR Spectroscopy Analyses of BSA and D-BSA

In order to investigate a variation in the secondary structure of BSA upon dopamine conjugation, ATR-FTIR analysis was performed (Figure 3.3). By ATR-FTIR analysis, amide bonds in protein were monitored. Amide I (~ 1640 cm^{-1}), II (~ 1530 cm^{-1}) and III (~ 1240 cm^{-1}) bands are the important IR characterizations of proteins (Liu et al. 2013; Kaiden et al. 1987). Amide I and amide II bands corresponds to C=O stretching vibrations and N-H bending vibrations, which are vibrations of C-N-H angles, respectively (Grdadolnik and Marécha, 2001). Upon dopamine conjugation, a detectable change was observed in the region of amide III at 1243 cm^{-1} due to a new amide bond formation (Kaiden et al., 1987).

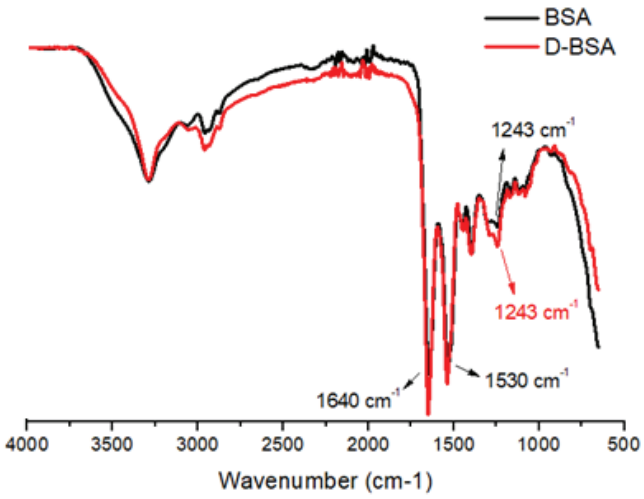

Figure 3.3. ATR-FTIR spectra of native BSA (black) and dopamine conjugated BSA (D-BSA) (red).

3.1.4. UV-Vis Spectroscopy Analyses of BSA and D-BSA

In this study, dopamine conjugation provides catechol groups to the surface of the BSA. If catechol groups are found as oxidized form named as quinone on BSA surface, required properties cannot be provided to the synthesized nanoparticles. To determine dopamine conjugation and the presence of catechol molecules, UV-Vis study was performed (Figure 3.4).

Absorption peak of catechol was observed at 280 nm due to its phenolic group and molar extinction coefficient of dopamine hydrochloride is 4,293 $mole^{-1}$ cm^{-1} (Murthy

and Sundaram, 1996). Characteristic absorption peak of BSA at 278 nm is coming from aromatic amino acids (tryptophan, tyrosine and phenylalanine). In a BSA, 2 tryptophan, 19 tyrosine and 27 phenylalanine are found (Chudzik et al., 2016). Molar extinction coefficients of tryptophan, tyrosine and phenylalanine are 5,540 $M^{-1}cm^{-1}$, 1,480 $M^{-1}cm^{-1}$ and 200 $M^{-1}cm^{-1}$, respectively (Mach et al., 1992). By dopamine conjugation, absorption peak of BSA was shifted to 277 nm and intensity of the peak increased. Blue shift of BSA peak is explained by disturbed tryptophan (Trp-134) which is found on BSA surface by catechol molecules. Since molar extinction coefficient of catechol is high and 15 dopamine molecules are found in BSA, increase in intensity of the peak indicates that D-BSA contains catechol molecules. It is also confirmed by UV-Vis measurement of dopamine as same concentration as on a D-BSA protein. When dopamine molecules conjugated with BSA, catechol peaks were also overlapped with absorption peak of BSA so, D-BSA had higher absorption peak compared to BSA. Also, absorbance peaks above 300 nm was not observed which shows that any of the catechol molecules were oxidized and formed quinone (Scalzone et al., 2020).

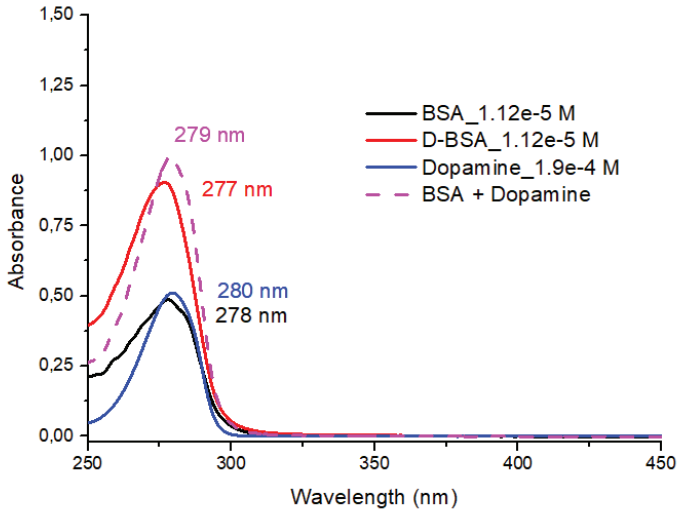

Figure 3.4. UV-Vis spectra of native BSA (black), dopamine conjugated BSA (D-BSA) (red) proteins dopamine (blue) and the sum of BSA and dopamine peaks (pink).

3.1.5. Fluorescence Spectroscopy Analyses of BSA and D-BSA

For BSA, the aromatic amino acids (tryptophan, tyrosine and phenylalanine) show fluorophore properties (Lakowicz, 2006). The absorption coefficient constants for tryptophan, tyrosine and phenylalanine are $5x10^3$ $M^{-1}cm^{-1}$, $2x10^3$ $M^{-1}cm^{-1}$, 0.25 $x10^3$ $M^{-1}cm^{-1}$, respectively (Lakowicz, 2006). Due to the high absorption constant of tryptophan and tyrosine, BSA is generally excited at wavelengths of 280 nm or longer. When the protein is excited at a wavelength of 280 nm, the spectrum shows tyrosine and tryptophan amino acids. However, when the protein is excited at wavelengths of 295 nm and longer, tyrosine is not stimulated and the spectrum shows tryptophan. There are 2 tryptophan amino acids named as Trp-214 located within a hydrophobic binding pocket of domain II and Trp-134 located on the surface of domain I in a BSA protein (Buddanavar and Nandibewoor, 2017).

Fluorescence emission spectra of BSA and D-BSA at different excitation wavelengths (278 nm and 295 nm) are shown in Figure 3.5. By dopamine conjugation, characteristic peak of BSA shows 13 nm blue shift and its intensity decreased. Trp-134 is located on the surface of the molecule, so Trp-134 is affected by surface modifications. Also, 25% of tyrosine residues are found on the surface of the BSA which may be also affected by additional fluorophores on BSA surface (Li et al. 2021). Since dopamine has also aromatic group, these groups may block tryptophan and tyrosine residues and cause quenching. Since blue shift was observed at two different excitation wavelengths, fluorophore concentration on sample increases, which shows dopamine conjugation on BSA surface.

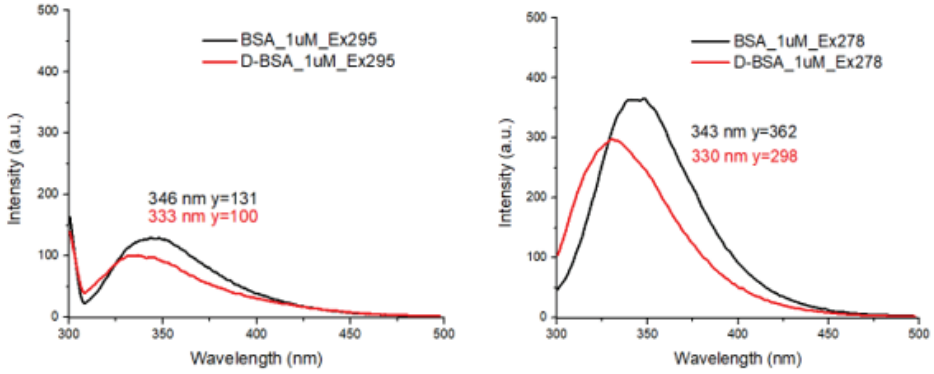

Figure 3.5. Fluorescence emission spectra of native BSA (black) and dopamine conjugated BSA (D-BSA) (red) proteins excitation at 295 nm (left) and 278 nm (right) in ultra-pure water.

3.1.6. Conformational and Antioxidant Studies of BSA and D-BSA

Serum albumin protein has seven fatty acid binding sites. By comparing fatty acid binding sites, the conformations of BSA and D-BSA can be analyzed. Bound and unbound spin labeled fatty acids can be identified by electron paramagnetic resonance (EPR) spectroscopy (Akdogan and Hinderberger, 2011; Akdogan et al., 2011; Bhattacharya, 2020). Due to the restricted rotational motion of bound fatty acids, they have broad EPR signals while unbound fatty acids have sharp EPR signals due to freely tumbling motion (Akdogan and Hinderberger, 2011; Akdogan et al., 2011). Figure 3.6(A) showed that spin labeled fatty acids, 16-doxyl stearic acid (16-DSA), were bound to binding sites of both BSA and D-BSA, similarly.

All broad signals originated from restricted rotational motion of bound fatty acids were observed up to seven fatty acids per protein. This result can be concluded that functionalization of protein surface with dopamine did not change the fatty acid binding sites of BSA and thus the conformation of BSA, significantly.

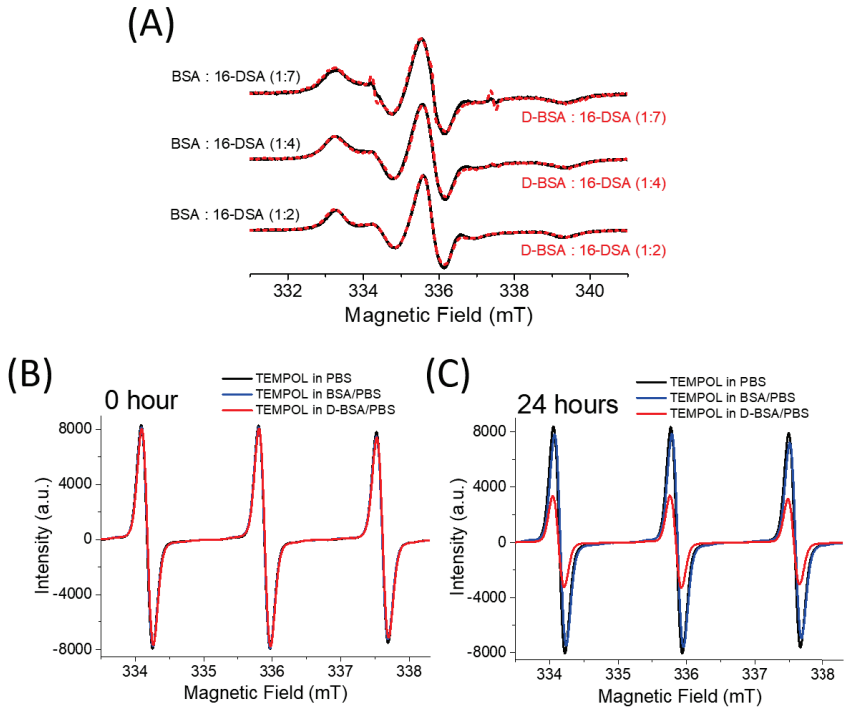

Figure 3.6. (A) EPR spectra of 16-DSA (1.5 mM) upon binding to BSA (black) and D-BSA (red) at different ratios 1:2, 1:4 and 1:7, BSA (or D-BSA):16-DSA. (B, C) EPR spectra of TEMPOL (0.7 mM) in PBS (black), BSA/PBS (blue) and D-BSA/PBS (red) just after mixture (B) and after 24 hours of mixture (C). BSA (or D-BSA):TEMPOL ratio is 1:1.

Due to its catechol hydroxyl groups, dopamine has antioxidant properties (Kanazawa, 2000; Yen, 1997; Al-Mamary, 2020). Dopamine conjugation to albumin surface is expected to be gained antioxidant property to BSA. EPR spectroscopy can be used to compare the antioxidant activity of BSA surface before and after dopamine conjugation. For this aim, 4-hydroxy-2,2,6,6-tetramethylpiperidine-1-oxyl (TEMPOL) which is a nitroxide based spin radical can be used to determine the radical quenching effect of BSA and D-BSA. Figure 3.6(B) shows that EPR spectra of 0.7 mM TEMPOL in PBS, in BSA/PBS or in D-BSA/PBS have similar intensities (at BSA or D-BSA:TEMPOL ratio is 1:1) just after sample preparation (0 hour). After 24 h, the EPR signal of TEMPOL decreased by 60% in the presence of D-BSA (Figure 3.6(C)). On the other hand, addition of BSA did not affect the signal intensity of TEMPOL significantly. As a result, dopamine conjugation is improved antioxidant activity of serum albumin, considerably. Additionally, the antioxidant property of free dopamine was studied with TEMPOL in PBS buffer. The same amount of dopamine found in D-BSA was mixed with TEMPOL, and monitored with EPR spectroscopy just after sample preparation (0 hour) and after 24 hours. In the presence of free dopamine, the EPR signal of TEMPOL decreased by 43% after 24 hours (data not shown). These results show that dopamine antioxidant function is higher when dopamine is conjugated with BSA compared to free dopamine molecules. The weak interactions between TEMPOL and BSA support the interaction between dopamine and TEMPOL on BSA. Therefore, radical quenching ability of dopamine may increase when they are conjugated with BSA surface.

3.1.7. Stability of D-BSA in Water

Stability of synthesized D-BSA protein was determined by DLS measurements in terms of change in size, PDI and surface charge over time. For this aim, these parameters were measured through 21 days. In Figure 3.7, results showed that surface charge and size of the protein did not change, significantly. However, PDI value increased after 2 weeks which caused by oxidized catechol groups on D-BSA surface resulted protein crosslinking via disulfide groups, over time (Schweigert et al., 2001). Since size and surface charge did not show notable change, cross-linking of protein is limited and did not affect stability of D-BSA protein.

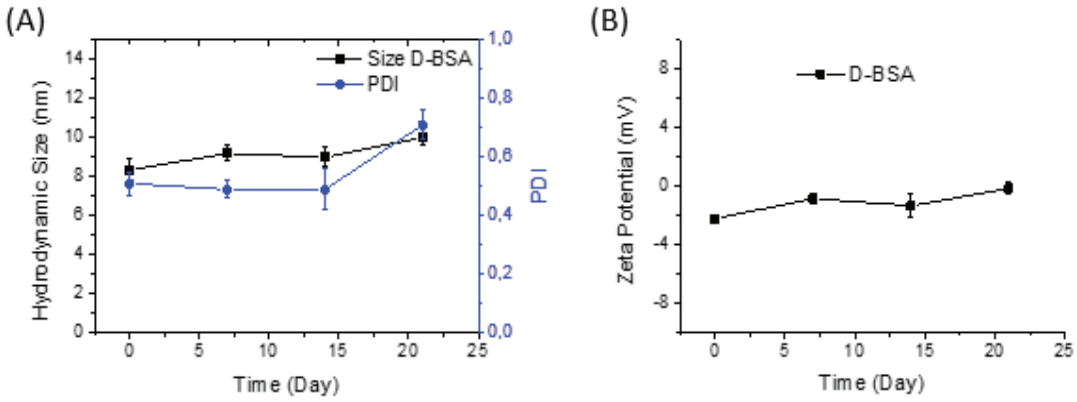

Figure 3.7. Hydrodynamic size distributions (A) and zeta potentials (B) of D-BSA protein.

3.2. Characterization of D-BSA NPs and DOX Loading

For producing dopamine conjugated BSA nanoparticles (D-BSA NPs), desolvation method was used. As desolvating agent, acetone:water (4:1)(v/v) was used in the desolvation process followed by the addition of VCl_3 as crosslinking agent. Other desolvating agents such as methanol, ethanol, propanol and acetonitrile were also applied. However, all of D-BSA protein were agglomerated and turbidity lost, completely. Only acetone:water (4:1, v:v) mixture provides high nanoparticle formation yield (65 ± 5%).

By using Dynamic Light Scattering (DLS) technique, the particle sizes of the obtained nanoparticle were evaluated in water. The mean hydrodynamic sizes of D-BSA NPs by using the desolvation method were found to be between 180 to 600 nm with a maximum peak at 294 nm. The polydispersity index (PDI) was 0.15 less than 0.2 indicate that homogeneous size distribution was obtained. (Figure 3.8 (A)). From zeta potential measurements, the surface charge of D-BSA NPs was found to be between -17 to -50 mV with an average and a maximum peak at -36 mV (Figure 3.8 (B)). High surface charge provides that NPs are repelling each other and indicate that NPs are highly stable and prevented from agglomeration.

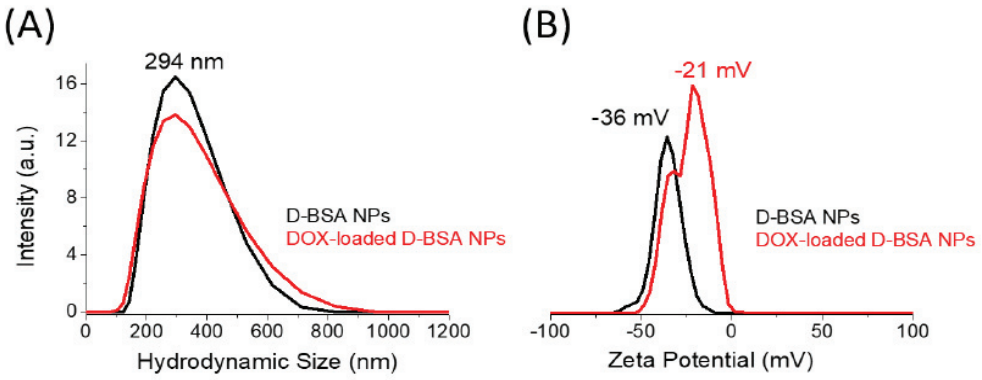

Figure 3.8. (A) DLS results of hydrodynamic size distributions and (B) zeta potentials of D-BSA NPs (black) and DOX loaded D-BSA NPs (red) in water. PDI values are 0.15 and 0.16 for D-BSA NPs and DOX loaded D-BSA NPs, respectively.

In Figure 3.9 (A, B), SEM images show that D-BSA NPs are formed as spherical shape. Since nanoparticles have small PDI value, agglomeration in Figure 3.9 (A) is observed due to the sample preparation requirement of SEM analyze which includes drying of NP droplets. Particle size distribution obtained from the SEM image showed 253 nm average size with a size distribution between 100 and 400 nm (Figure 3.9 (C)). Compared to DLS results, smaller particle size obtained by SEM can be explained by swelling of protein nanoparticles with water for DLS measurements.

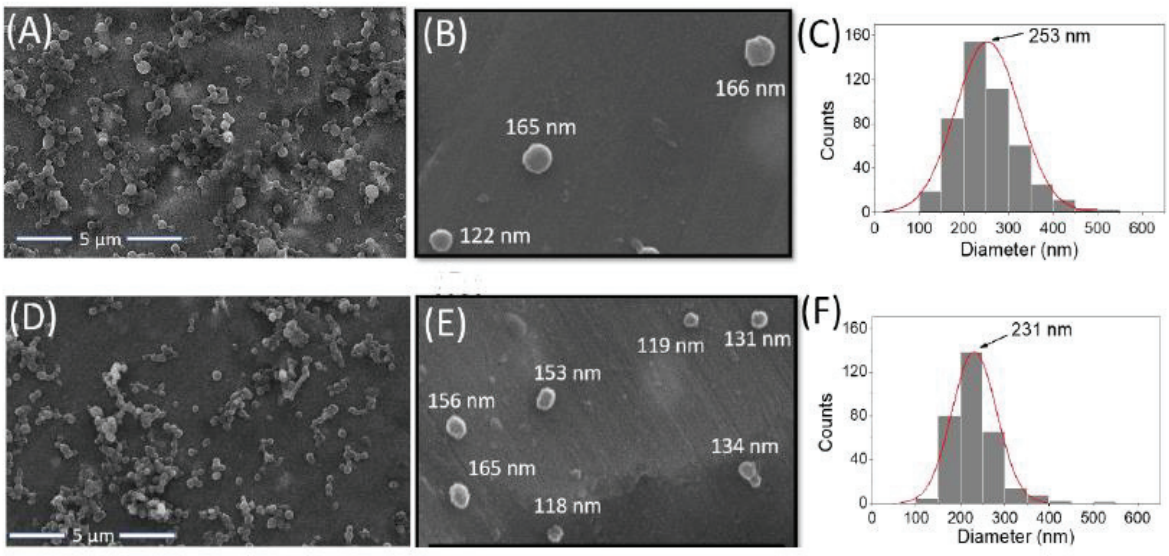

Figure 3.9. (A, B) SEM images of D-BSA NPs, (C) particle size distribution obtained from the SEM image (A), (D, E) SEM image of DOX loaded D-BSA NPs, (F) particle size distribution of DOX loaded D-BSA NPs obtained from the SEM image (D).

Doxorubicin (DOX) an anticancer drug was used to determine drug loading capacity of D-BSA NPs. There are two methods for drug loading into a NPs; desolvation and incubation. Drug can be added during desolvation process on protein solution or it can be incubated with NPs. Adding DOX during desolvation technique, dramatically decrease yield of the nanoparticle formation and NPs did not formed at high drug concentration ratio e.g., 15:1 (DOX:D-BSA) so, incubation method is preferred. Firstly, D-BSA NPs was synthesized then, incubated with DOX. For 15:1 DOX:D-BSA molar ratio, DOX encapsulation efficiency and drug loading capacity of D-BSA NPs were found to be 98% and 10.3%, respectively. DLS results (Figure 3.8 (A)) and SEM images (Figure 3.9 (D, E)) showed that DOX loading did not cause significant change in size and distribution of D-BSA NPs. Particle size distribution obtained from the SEM image showed 231 nm average size with a size distribution between 100 and 400 nm (Figure 3.9 (F)). However, the maximum zeta potential of D-BSA NPs surface shifted from -36 mV to -21 mV due to the surface coverage by DOX (Figure 3.9 (B)). Due to the hydrophobic aromatic base, polar hydroxyl and polar amino groups in DOX, it binds to NPs by both hydrophilic and hydrophobic interactions. Since surface charge became less negatively charged by DOX loading, decreasing of surface charge can be attributed to the polar interactions between DOX (hydroxyl and amine groups) and the surface of NPs which also shows polar property with -36 mV surface charge. Additionally, the interior of the nanoparticle has a hydrophobic structure and allows the penetration of DOX through hydrophobic interactions between aromatic base of DOX and proteins. Therefore, drugs loaded inside the nanoparticle showed a sustained slow release at pH 7.4 after rapid release of surface-bound drugs (Figure 3.12).

3.2.1. Stability of D-BSA NPs and DOX Loaded D-BSA NPs

In water, spherical NPs are not decomposed and they are dispersed, easily. Since pH of the water is neutral (pH:7.0), water also provide stable environment for pH responsive D-BSA NPs. The colloidal suspension of D-BSA NPs in water was obtained due to the large negative surface potential of the NPs which is between -17 to -50 mV with an average and a maximum peak at -36 mV (Figure 3.8. (A) DLS results of hydrodynamic size distributions and (B) zeta potentials of D-BSA NPs (black) and DOX loaded D-BSA NPs (red) in water. PDI values are 0.15 and 0.16 for D-BSA NPs and

DOX loaded D-BSA NPs, respectively.Aspartic and glutamic acid negatively charged amino acids on the NPs provides polar anionic surface. Therefore, electrostatic repulsive forces between anionic NPs as well as hydration layers around the polar surface of NPs keep them apart and avoids particle agglomeration. Yet, increasing the concentration of NPs above 0.5 mg/mL causes agglomeration with time and subsequent precipitation. However, they can be resuspended within minutes by using vortex mixing.

The structural stability of D-BSA NPs and DOX-loaded D-BSA NPs in water were studied using DLS and zeta potential measurements. In Figure *3.10*, the hydrodynamic sizes and surface potentials of these materials did not change significantly over 3 weeks which shows the stability of NPs. Only the mean zeta potential value of DOX-loaded D-BSA NPs changed from -25 mV average to -35 mV over time due to possible drug release from the surface of the NPs.

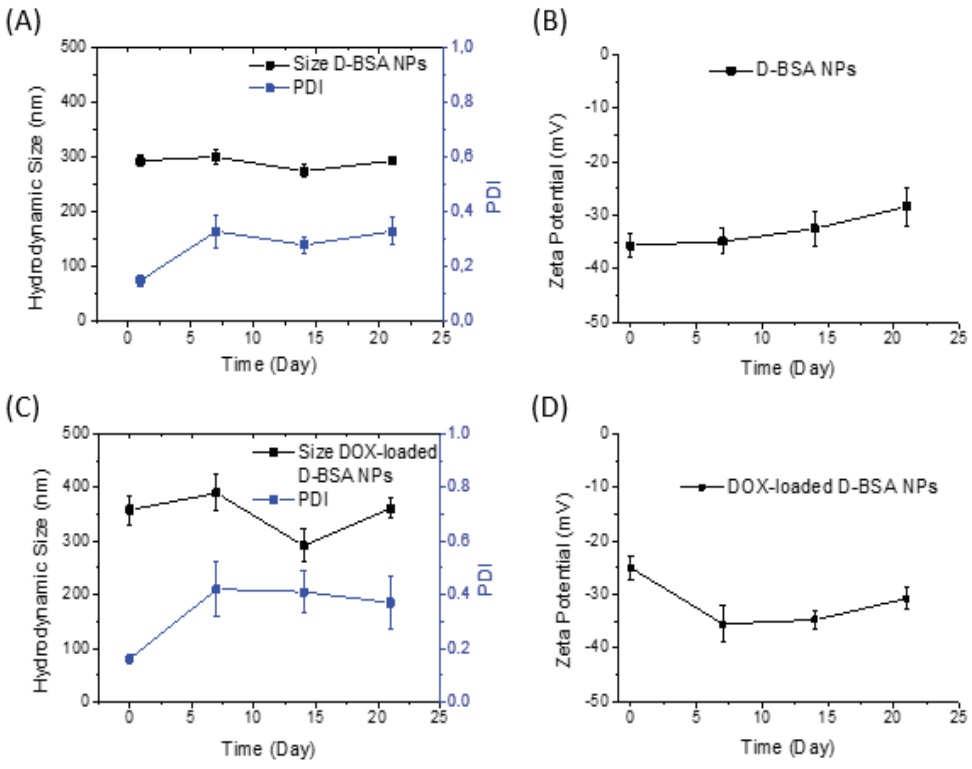

Figure 3.10. DLS results of hydrodynamic size distributions and zeta potentials of D-BSA NPs (A, B), DOX-loaded D-BSA NPs (C, D) in water within 21 days.

3.2.2. pH Sensitivity of D-BSA NPs

By the catechol-V(III) coordination bond, D-BSA NPs have a pH sensitive property. V(III) ions provide tris- coordination bonds at pH 8.0 before the catechol oxidation, predominantly. Transition of mono- catechol-V(III) complex to bis- and eventually tris- catechol-V(III) complexes by addition of NaOH using UV-Vis absorption spectroscopy was shown (Sever and Wilker, 2004). Under argon gas, addition of 2 equivalent NaOH per V(III) ions (corresponding pH value is about 4.5) yielded mono complexes (425 and 467 nm), 4 equivalent NaOH (corresponding pH value is about 7.0) yielded bis complexes (402 and 635 nm) and 5 equivalent NaOH (corresponding pH value is about 10.0) yielded tris complexes (361, 600 and 650 nm). On the other hand, Holten-Andersen et al. monitored mono- bis- and tris- coordination bonds by Raman spectroscopy and showed that a higher rate of tris- catechol-V(III) coordination was obtained compared to bis- and mono- types at pH 8.0 (Holten-Andersen, 2014). Therefore, in order to prevent catechol oxidation and obtaining tris- coordination, concurrently, D-BSA NPs was synthesized at pH between 7.4 and 8.0. For the determination of tris-, bis- and mono- complexes at different pH values, UV-Vis spectroscopy can be used but the continuous absorption signal of BSA aggregates synthesized in the acetone-water mixture by desolvation inhibited detection of mono-, bis- and tris- catechol-V(III) coordination signals. Therefore, the same procedure for NP formation was applied with dopamine molecules and V(III) ions. Dopamine:V(III) were mixed at a 3:1 molar ratio at pH 4.2, 5.5 and 8.0 under argon gas, and measured by UV-Vis absorption spectroscopy (Figure 3.11 (A)). At pH 4.2, The main absorption signal at 470 nm corresponds to the mono- catechol-V(III) complex. When pH of the complex was increased, this signal shifts to lower wavelength 425 nm and 350 nm at pH 5.5 and 8.0, respectively. In addition, increasing the pH values to 5.5 and 8.0 caused new broad signals between 550 – 850 nm indicates bis- and tris- coordination.

In order to study the effect of pH on the structure, D-BSA NPs were dissolved in PBS (0.01 M) at different pH values e.g. 4.2, 5.5 and 7.4 and suspended in buffered solution overnight and measured by DLS. The maximum intensity at the particle size distribution was shifted from 210 nm to 342 and 530 nm in PBS buffer at pH 7.4, 5.5 and 4.2, respectively (Figure 3.11

(B)). When pH value decreases, size of NPs increases due to the breaking of crosslinking, because tris- coordination transformed to bis- and/or mono- coordination. In addition, lowering the pH of the PBS solution increase in PDI values from 0.28 to 0.41 and 0.59 at pH 7.4, 5.5 and 4.2, respectively. Less uniform size distribution was observed with decreasing pH. The zeta potentials of D-BSA NPs were found to be similar at pH 7.4 and 5.5, but the absolute value of zeta potential decreased from -28 mV to -20 mV at pH 4.2 due to greater protonation in more acidic solution.

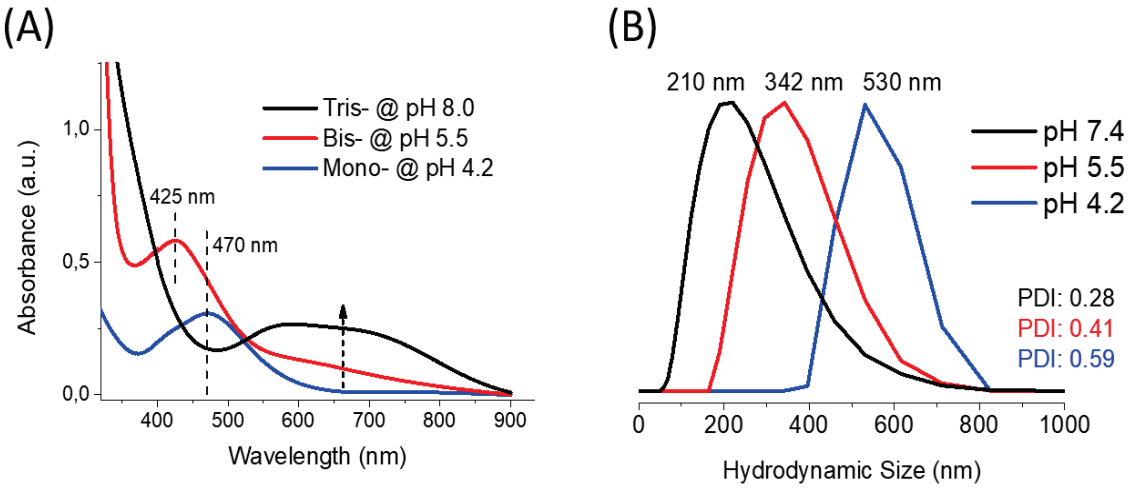

Figure 3.11. (A) UV-Vis absorption spectra of dopamine and V(III) mixture at different pH values: 8.0 (black), 5.5 (red) and 4.2 (blue) under argon gas. (B) DLS results of hydrodynamic size distributions of D-BSA NPs in PBS buffer at different pH values: 7.4 (black), 5.5 (red) and 4.2 (blue). PDI values are 0.28, 0.41 and 0.59 for pH (black), 5.5 (red) and 4.2 (blue), respectively.

3.2.3. In Vitro Release Studies of DOX from D-BSA NPs

The drug releasing ability of D-BSA NPs depends on the pH sensitivity. Release dynamics of DOX from the NPs was observed at different pH values (Figure 3.12). At acidic pH, mono- and bis- catechol-V(III) complexes will predominate in NPs structure, so the drug release rate as well as the cumulative amount of released drug are expected to be higher compared to physiological pH, which averages 7.4. In the first 8 hours of drug release monitoring, the cumulative DOX releases were found to be 33, 41 and 75%, at pH values 7.4, 5.5 and 4.2, respectively. After 8 hours, the rate of drug release decreased but

at the end of 80 hours total DOX releases reached to 53, 75 and 90% at pH values 7.4, 5.5 and 4.2, respectively. At pH 4.2, since mono- catechol-V(III) complex formation causes breaking crosslinking bonds, drug release (up to 90%) increased, dramatically. At pH 7.4 and 5.5, the difference in the amounts of releases (53 and 74%, after 80 hours) indicate that conversion of tris- complexes at pH 7.4 to bis- complexes at pH 5.5. As a result, DOX release from D-BSA NPs depends on the formation of tris- complex structure under physiological conditions, but rapid release observed at lower pH.

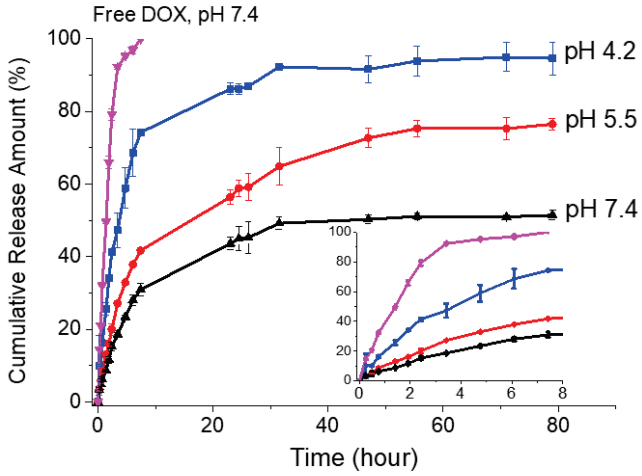

Figure 3.12. Cumulative release amount of DOX from D-BSA NPs in 0.01 M PBS buffer at 37 ^{0}C at pH 7.4 (black), pH 5.5 (red) and pH 4.2 (blue). As a reference measurement, the release rate of the same amount of free DOX was also performed (pink). The initial 8 hours of DOX release amounts from all samples were displayed in the inset of Figure (C).

3.3. Cellular uptake of D-BSA NPs and their effects on the cell viability in vitro

Breast cancer cell line, MCF-7, was chosen for the studies of the cellular uptake of NPs and their effects on the cell viability. In order to visualize their uptake and distribution in cells, fluorescein isothiocyanate (FITC) labeled BSA proteins were used. FITC-labeled BSA proteins were conjugated with dopamines, and then mixed with D-BSA with a 1:4 ratio before the NP preparation. 0.075 mg/mL of DOX-loaded or unloaded FITC-labeled D-BSA NPs were incubated with MCF-7, for 24 hours. Both NPs were observed in the MCF-7 cells

(Figure 3.13 (A, B)). The mechanism of internalization was not investigated here, however endocytic or gp60 receptor medicated uptake of serum albumin nanoparticles has been documented in the literature. Endocytic uptake of negatively charged serum albumin NPs has been shown via both caveolae or clathrin mediated endocytosis pathways using inhibitors of filipin and chlorpromazine, respectively (Desai et al., 2006; Komiya et al., 2016).

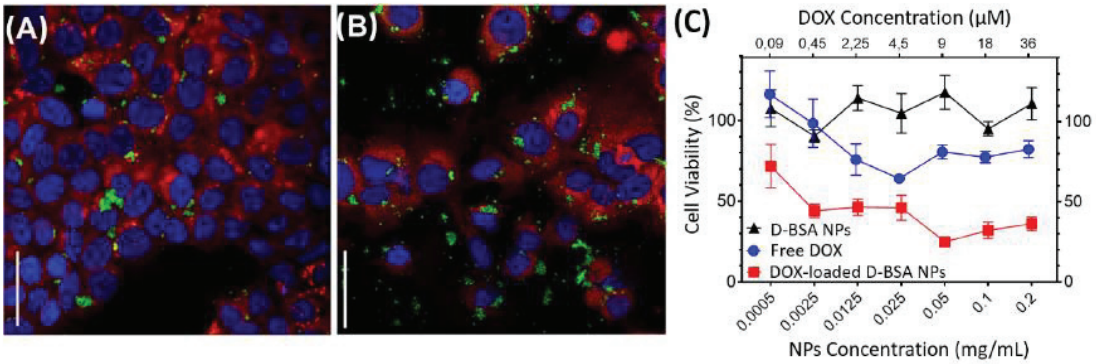

Figure 3.13. Confocal microscope images (40X) of MCF-7 cells treated with 0.075 mg/mL of unloaded (A) or DOX-loaded (B) FITC-labeled D-BSA NPs (green) for 24 hours. Cells membranes were stained with Dil (red) live cell dye and nuclei were stained with DAPI (blue). Scale bar = 50 μm. (C) The percentages of MCF-7 viability upon additions of different concentrations of D-BSA NPs (black), free DOX (blue) or DOX-loaded D-BSA NPs after 24 hours incubation time.

The cytotoxicity of prepared D-BSA NPs, were tested in both MCF-7 and cells, with MTT test after 24 hours incubation with NPs. Figure 3.13 (C) shows that increasing D-BSA NPs concentrations up to 0.1 mg/mL does not affect the viability of MCF-7 cells significantly (black line). The half-maximal inhibitory concentration (IC_{50}) value of V(III) ion has been reported as 70 μM in the literature (Kamphorst et al., 2015). The weight ratio of V(III) in D-BSA NPs was found to be 0.003% by the use of ICP-MS. This shows that only 0.8% of conjugated dopamine is cross-linked with V(III) ions to form tris- catechol-V(III) coordination in D-BSA NPs. As a result, the concentration of V(III) ions used in the formation of tris- catechol-V(III) coordination in 0.1 mg/mL D-BSA NPs was found to be 0.06 μM which is much lower than the IC_{50} value of V(III) (70 μM) (Kamphorst et al., 2015). Therefore, V(III) ion used in the preparation of BSA NPs is not expected to induce any toxicity to cells.

The anticancer drug of DOX acts in the cancer cell through DNA damage after intercalation with DNA, poisoning of topoisomerase-II enzyme and formation of free radicals that damage DNA, cellular membranes and proteins (Thorn et al., 2011). Addition of free DOX to MCF-7 cells resulted in a decrease of cell viability by 20% in the range of 2.25 – 36 μM of DOX concentration (Figure 3.13 (C)). However, addition of DOX-loaded D-BSA NPs decreased the cell viability more efficiently. Upon addition of 0.05 mg/mL of DOX-loaded D-BSA NPs (carrying 9 μM of DOX), the cell viability decreased by 75%. Above this concentration, cell viability did not change significantly. To sum up, the killing effect of DOX on MCF-7 cell viability was significantly increased when DOX was given with D-BSA NPs, whereas unloaded D-BSA NPs had no toxicity.

CHAPTER 4

CONCLUSIONS

In this study, pH responsive serum albumin NPs were prepared by catechol-V(III) complex formation. BSA protein was functionalized by an average of fifteen catechol containing dopamine (D) molecules. D-BSA proteins were desolvated with acetone-water mixture, and then aggregated proteins were crosslinked by using VCl_3 which is V(III) ion containing metal salt. Tris- catechol-V(III) complex formation was achieved in the pH between 7.4 and 8.0 to prepare D-BSA NPs. For metal coordination complex, Fe(III) ions are commonly used. However, tris- catechol-V(III) complex formation can be predominated at relatively lower pH values compared to the pH value of tris- catechol-Fe(III) complex formation (pH 9.0). Thus, working with V(III) provides tris- coordination complex at lower pH values, so catechol groups are protected from oxidation and leads to the formation of uniformly sized NPs with an average of 253 nm according to SEM images.

pH sensitive catechol-V(III) coordination bonds allowed NP formation at pH between 7.4 and 8.0, but degraded them at acidic pH values: 5.5 and 4.2. Tris- catechol-V(III) coordination provided compact D-BSA NPs in the PBS buffer at pH 7.4 which is 210 nm by using DLS measurements. At lower pH values, maximum intensity of the particle size distribution increased to 342 and 530 nm when the pH values of PBS buffer medium changed to 5.5 and 4.2, respectively. It can be explained by opening structures of pH responsive NPs at lower pH values. In addition, decreasing pH value increased the PDI values of the NPs from 0.28 to 0.41 and 0.59 at pH 7.4, 5.5 and 4.2, respectively.

In order to show the pH responsive property of the obtained NPs, drug release profile of NPs at medium with different pH values was also studied. In the first 8 hours, the drug release rate was slow and limited to 31% at pH 7.4, while it reached to 42% and 75% at pH 5.5 and 4.2, respectively. Also, total DOX releases reached to 51, 76 and 95% at pH values 7.4, 5.5 and 4.2, respectively at the end of 80 hours.

In brief, obtaining smaller NPs with a lower PDI value, and having slow and limited drug release could be explained by the presence of tris- catechol-V(III) complexes at pH 7.4. When pH decreased to 5.5 and 4.2, the size and PDI value of NPs increased,

and also the release of drug became faster and higher due to the conversion of tris-complexes to bis- and mono- complexes, respectively.

For unloaded and DOX-loaded NPs, cell entry of NPs were similar. Even at relatively low concentration, both were uptaken by cells, efficiently. Due to cell viability test, synthesized D-BSA NPs are not toxic to cells. In addition, DOX-loaded D-BSA NPs showed higher cytotoxicity, the cell viability decreased by 75%, compared to the treatment with the same concentration of free DOX (decreased by 20%). These results show that the easy cell uptake of D-BSA NPs enabled DOX induced cytotoxicity.

REFERENCES

Agudelo, D., Bourassa, P., Bérubé, G., Tajmir-Riahi, T. H., Intercalation of antitumor drug doxorubicin and its analogue by DNA duplex: Structural features and biological implication, International Journal of Biological Macromolecules, 66 (2014), 144–150.

Akdogan, Y. and Hinderberger, D., Solvent-induced protein refolding at low temperatures, J. Phys. Chem. B 115 (2011), 15422–15429.

Akdogan, Y., Emrullahoglu, M., Tatlidil, D., Ucuncu, M., Cakan-Akdogan, G., EPR studies of intermolecular interactions and competitive binding of drugs in a drug–BSA binding model, Physical Chemistry Chemical Physics, 18(32) (2016), 22531-22539.

Akdogan, Y., Junk, M. J. N., Hinderberger, D., Effect of ionic liquids on the solution structure of human serum albumin, Biomacromolecules, 12 (2011), 1072–1079.

Akdogan, Y., Reichenwallner, J., Hinderberger, D., Evidence for Water-Tuned Structural Differences in Proteins: An Approach Emphasizing Variations in Local Hydrophilicity, PLOS ONE, 7 (2012), e45681.

Akdogan, Y., Sozer, S. C., Akyol, C., Basol, M., Karakoyun, C., Cakan-Akdogan, G., Synthesis of albumin nanoparticles in a water-miscible ionic liquid system, and their applications for chlorambucil delivery to cancer cells, J. Mol. Liq., 367 (2022), 120575.

Akdogan, Y., Wei, W., Huang, K. Y., Kageyama, Y., Danner, E. W., Miller, D. R., Han, S., Intrinsic surface-drying properties of bioadhesive proteins, Angewandte Chemie, 126(42) (2014), 11435-11438.

Al-Mamary, M. A., Moussa, Z., Antioxidant Activity: The presence and impact of hydroxyl groups in small molecules of natural and synthetic origin. Antioxidants - benefits, sources, mechanisms of action, IntechOpen. (2021), p 729.

Amighi F. And Djomeh Z.E., Effect of different cross-linking agents on the preparation of bovine serum albumin nanoparticles, Journal of the Iranian Chemical Society, 17 (2020), 1223–1235.

Andersen, A., Krogsgaard, M., Birkedal, H., Mussel-inspired self-healing double-cross-linked hydrogels by controlled combination of metal coordination and covalent cross-linking, Biomacromolecules, 19(5) (2017), 1402-1409.

Anselmo, A. C. and Mitragotri, S., Nanoparticles in the clinic: An update, Bioengineering & translational medicine, 4(3) (2019), e10143.

Argitekin, E., Ersoz-Gulseven, E., Cakan-Akdogan, G., Akdogan, Y., Dopamine-conjugated bovine serum albumin nanoparticles containing pH-responsive catechol-V (III) coordination for in vitro and in vivo drug delivery, Biomacromolecules, 24(8) (2023), 3603-3618.

Ayad, M. I., Synthesis, characterization and catechol oxidase biomimetic catalytic activity of cobalt (II) and copper (II) complexes containing N_2O_2 donor sets of imine ligands, Arabian Journal of Chemistry, 9 (2016), S1297-S1306.

Aziz, A., Sefidbakht, Y., Rezaei, S., Kouchakzadeh, H., Uskoković, V., Doxorubicin-loaded, pH-sensitive albumin nanoparticles for lung cancer cell targeting, Journal of Pharmaceutical Sciences, 111(4) (2022), 1187-1196.

Barbosa, L. R., Ortore, M. G., Spinozzi, F., Mariani, P., Bernstorff, S., Itri, R., The importance of protein-protein interactions on the pH-induced conformational changes of bovine serum albumin: a small-angle X-ray scattering study, Biophysical journal, 98(1) (2010), 147-157.

Behzadi, S., Serpooshan, V., Tao, W., Hamaly, M. A., Alkawareek, M. Y., Dreaden, E. C., Brown, D., Alkilany, A. M., Farokhzad, O. C., Mahmoudi, M., Cellular Uptake of NPs: Journey Inside the Cell, Chem. Soc. Rev. 46 (14) (2017), 4218–4244.

Bhattacharya, A. A., Grune, T., Curry, S., Crystallographic analysis reveals common modes of binding of medium and long-chain fatty acids to human serum albumin, J. Mol. Biol. 303 (2000), 721–732.

Bilotto, P., Labate, C., De Santo, M. P., Deepankumar, K., Miserez, A., Zappone, B., Adhesive properties of adsorbed layers of two recombinant mussel foot proteins with different levels of DOPA and tyrosine, Langmuir, 35(48) (2019), 15481-15490.

Buddanavar, A. T. and Nandibewoor, S. T., Multi-spectroscopic characterization of bovine serum albumin upon interaction with atomoxetine. Journal of pharmaceutical analysis, 7(3) (2017), 148-155.

Cakan-Akdogan, G., Ersoz, E., Sozer, S. C., Gelinci, E., An in vivo zebrafish model reveals circulating tumor cell targeting capacity of serum albumin nanoparticles, J. Drug Deliv. Sci. Technol., 75 (2022), 103658. .

Calcinotto, A., Filipazzi, P., Grioni, M., Lero, M., De Milito, A., Ricupito, A., Cova, A., Canese, R., Jachetti, E., Rossetti, M., Huber, V., Parmiani, G., Generoso, L., Santinami, M., Borghi, M., Fais, S., Bellone, M., Rivoltini, L., Modulation of microenvironment acidity reverses anergy in human and murine tumor-infiltrating T lymphocytes. Cancer Res. 72 (2012), 2746–2756.

Chaiwaree, S., Prapan, A., Suwannasom, N., Laporte, T., Neumann, T., Pruß, A., Bäumler, H., Doxorubicin–loaded human serum albumin submicron particles: preparation, characterization and in vitro cellular uptake, Pharmaceutics, 12(3) (2020), 224.

Chamundeeswari, M., Jeslin, J., Verma, M. L., Nanocarriers for drug delivery applications. Environmental Chemistry Letters, 17(2) (2019), 849-865.

Chatterjee, K., Zhang, J., Honbo, N., Karliner, J. S., Doxorubicin cardiomyopath, Cardiology, 115 (2010), 155-162.

Chen, B., He, X. Y., Yi, X. Q., Zhuo, R. X., Cheng, S. X., Dual-peptide-functionalized albumin-based nanoparticles with ph-dependent self-assembly behavior for drug delivery. ACS applied materials & interfaces, 7(28) (2015), 15148-15153.

Chen, H., Liu, D., Guo, Z., Endogenous stimuli-responsive nanocarriers for drug delivery, Chemistry Letters, 45(3) (2016), 242-249.

Cheng, K., Sun, S., Gong, X., Preparation, characterization, and antiproliferative activities of biotin-decorated docetaxel-loaded bovine serum albumin nanoparticles. Braz. J. Pharm. Sci., 54(2) (2018), e17295.

Cheng, Z., Yan, M., Cao, L., Huang, J., Cao, X., Yuan, D., Chen, Y., Design of nitrile rubber with high strength and recycling ability based on Fe^{3+}-catechol group coordination, Industrial & Engineering Chemistry Research, 58(9) (2019), 3912-3920.

Choi, S. Y. C., Collins, C. C., Gout, P. W., Wang, Y., Cancer-generated lactic acid: a regulatory, immunosuppressive metabolite? J. Pathol., 230 (2013), 350-355.

Chudzik, M., Maciążek-Jurczyk, M., Pawełczak, B., Sułkowska, A., Spectroscopic studies on the molecular ageing of serum albümin, Molecules, 22(1) (2016), 34.

Croissant, J. G., Fatieiev, Y., Khashab, N. M., Degradability and clearance of silicon, organosilica, silsesquioxane, silica mixed oxide, and mesoporous silica nanoparticles, Advanced materials, 29(9) (2017), 1604634.

Cuvier, C., Roblot-Treupel, L., Millot, J. M., Lizard, G., Chevillard, S., Manfait, M., Couvreur, P., Poupon, M. F., Doxorubicin-loaded nanospheres bypass tumor cell multidrug resistance, Biochemical Pharmacology, 44 (1992), 509–517.

Dalsin, J. L., Lin, L., Tosatti, S., Vörös, J., Textor, M., Messersmith, P. B., Protein resistance of titanium oxide surfaces modified by biologically inspired mPEG−DOPA, Langmuir, 21(2) (2005), 640-646.

Demirkurt, B., and Akdogan, Y., Development of an ionic liquid based method for the preparation of albumin nanoparticles, ChemistrySelect, 3(34) (2018), 9940-9945.

Desai, N.; Trieu, V.; Yao, Z.; Louie, L.; Ci, S.; Yang, A.; Tao, C.; De, T.; Beals, B.; Dykes, D.; Noker, P.; Yao, R.; Labao, E.; Hawkins, M.; Soon-Shiong, P. Increased antitumor activity, intratumor paclitaxel concentrations, and endothelial cell transport of cremophorfree, albumin-bound paclitaxel, ABI-007, compared with cremophor-based paclitaxel. Clin. Cancer Res., 12 (2006), 1317–1324.

Din, F. U., Aman, W., Ullah, I., Qureshi, O. S., Mustapha, O., Shafique, S., Zeb, A., Effective use of nanocarriers as drug delivery systems for the treatment of selected tumors, International journal of nanomedicine, vol. 12 (2017) 7291-7309.

Ding, D., Tang, X., Cao, X., Wu, J., Yuan, A., Qiao, Q., Hu, Y., Novel self-assembly endows human serum albumin nanoparticles with an enhanced antitumor efficacy, Aaps Pharmscitech, 15(1) (2014), 213-222.

Dreis, S., Rothweiler, F., Michaelis, M., Cinatl, J., Kreuter, J., Langer, K., Preparation, characterisation and maintenance of drug efficacy of doxorubicin-loaded human serum albumin (HSA) nanoparticles, International Journal of Pharmaceutics, 341 (2007), 207–214.

Eisele, K., Gropeanu, R. A., Zehendner, C. M., Rouhanipour, A., Ramanathan, A., Mihov, G., Koynov, K, Kuhlmann, C. R. W., Vasudevan, S. G., Luhmann, H., Weil, T., Fine-tuning DNA/albumin polyelectrolyte interactions to produce the efficient transfection agent cBSA-147, Biomaterials, 31(33) (2010), 8789-8801.

Ejima, H., Oba, A., & Yoshie, N., Tuning the mechanical properties of bioinspired catechol polymers by incorporating dual coordination bonds. Journal of Photopolymer Science and Technology, 31(1) (2018), 75-80.

Esfahlan, AJ., Dastmalchi, S., Davaran, S. A., Simple desolvation method for the rapid preparation of albumin nanoparticles. Int J Biol Macromol. 91 (2016), 703–9.

Fan, C., Fu, J., Zhu, W., Wang, D. A., A mussel-inspired double-crosslinked tissue adhesive intended for internal medical use, Acta biomaterialia, 33 (2016), 51-63.

Filippidi, E., Cristiani, T. R., Eisenbach, C. D., Waite, J. H., Israelachvili, J. N., Ahn, B. K., Valentine, M. T., Toughening elastomers using mussel-inspired iron-catechol complexes. Science, 358(6362) (2017), 502-505.

Fukuzawa, K., Saitoh, Y., Akai, K., Kogure, K., Ueno, S., Tokumura, A., Otagiri, M., Shibata, A., Antioxidant effect of bovine serum albumin on membrane lipid peroxidation induced by iron chelate and superoxide, Biochimica et Biophysica Acta (BBA)-Biomembranes, 1668(1) (2005), 145-155.

Gao, Y., Zhou, H., Liu, G., Wu, J., Yuan, Y., Shang, A., Tumor Microenvironment: Lactic Acid Promotes Tumor Development, J. Immunol. Res. (2022), 3119375.

Gessner, I., and Neundorf, I., Nanoparticles modified with cell-penetrating peptides: Conjugation mechanisms, physicochemical properties, and application in cancer diagnosis and therapy, International journal of molecular sciences, 21(7) (2020), 2536.

Ghuman, J., Zunszain, P. A., Petitpas, I., Bhattacharya, A. A., Otagiri, M., Curry, S., Structural basis of the drug-binding specificity of human serum albumin, Journal of molecular biology, 353(1) (2005), 38-52.

Goksel, Y. and Akdogan, Y., Increasing spontaneous wet adhesion of DOPA with gelation characterized by EPR spectroscopy, Materials Chemistry and Physics, 228 (2019), 124–130.

Grdadolnik, J. and Maréchal, Y., Bovine serum albumin observed by infrared spectrometry. I. Methodology, structural investigation, and water uptake, Biopolymers: Original Research on Biomolecules, 62(1) (2001), 40-53.

Gulyaev, A. E., Gelperina, S. E., Skidan, I. N., Antropov, A. S., Kivman, G. Y., Kreuter, J., Significant transport of doxorubicin into the brain with polysorbate 80-coated nanoparticles, Pharmaceutical Research, 16 (10) (1999), 1564–1569.

Hachem, K., Ansari, M. J., Saleh, R. O., Kzar, H. H., Al-Gazally, M. E., Altimari, U. S., Kianfar, E., Methods of chemical synthesis in the synthesis of nanomaterial and nanoparticles by the chemical deposition method: A review. BioNanoScience (2022), 1-26.

Han, J., Wang, Q., Zhang, Z., Gong, T., & Sun, X., Cationic bovine serum albumin based self-assembled nanoparticles as siRNA delivery vector for treating lung metastatic cancer, Small, 10(3) (2014), 524-535.

He, Y., Gao, S., Jubsilp, C., Rimdusit, S., Lu, Z., Reprocessable polybenzoxazine thermosets crosslinked by mussel-inspired catechol-Fe^{3+} coordination bonds, Polymer, 192 (2020), 122307.

Hebel, M., Gacanin, J., Lückerath, T., Ng, D. Y. W., Weil, T., Controlling polymer morphologies by intramolecular and intermolecular dynamic covalent iron(III)/catechol complexation—from polypeptide single chain nanoparticles to hydrogels, Macromol. Rapid Commun, 43 (2022), 2100413.

Heidarian, P., Kouzani, A. Z., Kaynak, A., Bahrami, B., Paulino, M., Nasri-Nasrabadi, B., Varley, R. J., Rational Design of Mussel-Inspired Hydrogels with Dynamic Catecholato− Metal Coordination Bonds, Macromolecular Rapid Communications, 41(23) (2020), 2000439.

Hermanson, G. T., Vaccines and immunogen conjugates. bioconjugate techniques, (2013), 839-865.

Holten-Andersen, N., Jaishankar, A., Harrington, M. J., Fullenkamp, D. E., DiMarco, G., He, L., McKinley, G. H., Messersmith, P. B., Lee, K. Y. C., Metal-coordination: using one of nature's tricks to control soft material mechanics, J. Mater. Chem. B, 2 (2014), 2467.

Honary, S., Jahanshahi, M., Golbayani, P., Ebrahimi, P., Ghajar, K., Doxorubicin-loaded albumin nanoparticles: formulation and characterization, Journal of nanoscience and nanotechnology, 10(11) (2010), 7752-7757.

Hong, S., Choi, D. W., Kim, H. N., Park, C. G., Lee, W., Park, H. H., Protein-based nanoparticles as drug delivery systems, Pharmaceutics, 12(7) (2020), 604.

Hornok, V., Serum albumin nanoparticles: Problems and prospects, Polymers, 13(21) (2021), 3759.

Iqbal, H., Yang, T., Li, T., Zhang, M., Ke, H., Ding, D., Chen, H., Serum protein-based nanoparticles for cancer diagnosis and treatment, Journal of controlled release, 329 (2021), 997-1022.

Janes, K. A., Fresneau, M. P., Marazuela, A., Fabra, A., Alonso, M. J., Chitosan nanoparticles as delivery systems for doxorubicin, Journal of Controlled Release, 73 (2001), 255–267.

Jeong, Y. K., and Choi, J. W., Mussel-inspired self-healing metallopolymers for silicon nanoparticle anodes, Acs Nano, 13(7) (2019), 8364-8373.

Jia, R., Teng, L., Gao, L., Su, T., Fu, L., Qiu, Z., Bi, Y., Advances in multiple stimuli-responsive drug-delivery systems for cancer therapy, International Journal of Nanomedicine, 16 (2021), 1525.

Jia, Z., Zeng, Y., Tang, P., Gan, D., Xing, W., Hou, Y., Lu, X., Conductive, tough, transparent, and self-healing hydrogels based on catechol–metal ion dual self-catalysis, Chemistry of Materials, 31(15) (2019), 5625-5632.

Kaiden, K., Matsui, T., Tanaka, S., A study of the amide III band by FT-IR spectrometry of the secondary structure of albumin, myoglobin, and γ-globulin, Applied spectroscopy, 41(2) (1987), 180-184.

Kamphorst, J. J., Nofal, M., Commisso, C., Hackett, S. R., Lu, W., Grabocka, E., Vander Heiden, M. G., Miller, G., Drebin, J. A., Bar-Sagi, D., Human pancreatic cancer tumors are nutrient poor and tumor cells actively scavenge extracellular protein. Cancer Res. 75 (2015), 544–553.

Kanazawa, K. and Sakakibara, H., High content of dopamine, a strong antioxidant, in cavendish banana, J. Agric. Food Chem., 48 (2000), 844-848.

Karami, E., Behdani, M., Kazemi-Lomedasht, F., Albumin nanoparticles as nanocarriers for drug delivery: Focusing on antibody and nanobody delivery and albumin-based drugs. Journal of Drug Delivery Science and Technology, 55 (2020), 101471.

Karami, K., Jamshidian, N., Hajiaghasi, A., Amirghofran, Z., BSA nanoparticles as controlled release carriers for isophethalaldoxime palladacycle complex; synthesis, characterization, in vitro evaluation, cytotoxicity and release kinetics analysis, New Journal of Chemistry, 44(11) (2020), 4394-4405.

Karewicz, A., Polymeric and liposomal nanocarriers for controlled drug delivery, Biomaterials for Bone Regeneration, (2014), 351–373.

Karimi, M., Eslami, M., Sahandi-Zangabad, P., Mirab, F., Farajisafiloo, N., Shafaei, Z., Hamblin, M. R., pH-Sensitive stimulus-responsive nanocarriers for targeted

delivery of therapeutic agents, Wiley Interdisciplinary Reviews: Nanomedicine and Nanobiotechnology, 8(5) (2016), 696-716.

Karimi, M., Eslami, M., Sahandi-Zangabad, P., Mirab, F., Farajisafiloo, N., Shafaei, Z., Hamblin, M. R., pH-Sensitive stimulus-responsive nanocarriers for targeted delivery of therapeutic agents, Wiley Interdisciplinary Reviews: Nanomedicine and Nanobiotechnology, 8(5) (2016), 696-716.

Kim, B. J., Cheong, H., Hwang, B. H., Cha, H. J., Mussel-inspired protein nanoparticles containing iron(III)–DOPA complexes for pH-responsive drug delivery, Angew. Chem. Int., Ed.54 (2015), 7318-7322.

Kimura, K., Yamasaki, K., Nishi, K., Taguchi, K., Otagiri, M., Investigation of anti-tumor effect of doxorubicin-loaded human serum albumin nanoparticles prepared by a desolvation technique, Cancer chemotherapy and pharmacology, 83 (2019), 1113-1120.

Kırpat, I., Goksel, Y., Karakus¸ E., Emrullahoglu, M., Akdogan, Y., Determination of force-free wet adhesion of mussel-inspired polymers to spin labeled surface, Materials Letters, 205 (2017), 48–51.

Komiya, K.; Nakamura, T.; Nakashima, C.; Takahashi, K.; Umeguchi, H.; Watanabe, N.; Sato, A.; Takeda, Y.; Kimura, S.; Sueoka-Aragane, N. SPARC is a possible predictive marker for albumin-bound paclitaxel in non-small-cell lung cancer. Onco. Targets Ther. 2016, 9, 6663–6668.

Kord Forooshani, P. and Lee, B. P., Recent approaches in designing bioadhesive materials inspired by mussel adhesive protein, Journal of Polymer Science Part A: Polymer Chemistry, 55(1) (2017), 9-33.

Lakowicz, J. R. (Ed.)., Principles of fluorescence spectroscopy., Boston, MA: springer US, (2006) pg. 531.

Langer K, Balthasar S., Vogel V., Dinauer H., Briesen H., Schubert D., Optimization of the preparation process for human serum albumin (HSA) nanoparticles, Int J Pharm., 275 (2003), 169–80.

Langer K., Anhorn, M. G., Steinhauser, I., Dreis, S., Celebi, D., Schrickel, I., Faust, S., Vogel, V., Human serum albumin (HSA) nanoparticles: Reproducibility of preparation process and kinetics of enzymatic degradation, Int. J. Pharm., 347(1-2) (2008), 109-117.

Lee, H. J., Park, H. H., Sohn, Y., Ryu, J., Park, J. H., Rhee, W. J., Park, T. H., α-Galactosidase delivery using 30Kc19-human serum albumin nanoparticles for effective treatment of Fabry disease, Applied microbiology and biotechnology, 100 (2016), 10395-10402.

Leo, E., Cameroni, R., Forni, F., Dynamic dialysis for the drug release evaluation from doxorubicin-gelatin nanoparticle conjugates, International Journal of Pharmaceutics, 180 (1) (1999), 23-30.

Li, C. H., and Zuo, J. L., Self-healing polymers based on coordination bonds, Advanced Materials, 32(27) (2020), 1903762.

Li, H., Zhao, Y., Jia, Y., Qu, C., Li, J., Covalently assembled dopamine nanoparticle as an intrinsic photosensitizer and pH-responsive nanocarrier for potential application in anticancer therapy, Chemical Communications, 55(100) (2019), 15057-15060.

Li, M., Zhao, G., Su, W. K., Shuai, Q., Enzyme-responsive nanoparticles for anti-tumor drug delivery. Frontiers in Chemistry, 8 (2020), 647.

Li, S., Chen, Y., Zhu, W., Yang, W., Chen, Z., Song, J., Song, X., Chen, X., Yang, H., Engineered nanoscale vanadium metallodrugs for robust tumor-specific imaging and therapy, Adv. Funct. Mater., (2021), 2010337.

Li, Z., Wan, C., Liu, X., Wang, L., & Lee, D. J., Understanding of the mechanism of extracellular polymeric substances of aerobic granular sludge against tetracycline from the perspective of fluorescence properties, Science of The Total Environment, 756 (2021), 144054.

Liu, X., Shang, Y., Ren, X., Li, H., Molecular modeling and spectroscopic studies on the interaction of transresveratrol with bovine serum albumin. Journal of Chemistry, (2013), 7 pages.

López-Dávila, V., Seifalian, A. M., Loizidou, M., Organic nanocarriers for cancer drug delivery, Current opinion in pharmacology, 12(4) (2012), 414-419.

Lu, L., Tian, T., Wu, S., Xiang, T., Zhou, S., A pH-induced self-healable shape memory hydrogel with metal-coordination cross-links, Polymer Chemistry, 10(15) (2019), 1920-1929.

Lu, Q., Danner, E., Waite, J. H., Israelachvili, J. N., Zeng, H., Hwang, D. S., Adhesion of mussel foot proteins to different substrate surfaces, Journal of Royal Society Interface, 10 (2013), 20120759.

Lu, W., Zhang, Y., Tan, Y. Z., Hu, K. L., Jiang, X. G., Fu, S. K., Cationic albumin-conjugated pegylated nanoparticles as novel drug carrier for brain delivery, Journal of controlled release, 107(3) (2005), 428-448.

Lukyanov, A. N., Elbayoumi, T. A., Chakilam, A. R., Torchilin, V. P., Tumor-targeted liposomes: doxorubicin-loaded long-circulating liposomes modified with anti-cancer antibody, Journal of Controlled Release, 100 (2004), 135–144.

Ma, L., Qin, H., Cheng, C., Xia, Y., He, C., Nie, C., Zhao, C., Mussel-inspired self-coating at macro-interface with improved biocompatibility and bioactivity via dopamine grafted heparin-like polymers and heparin, Journal of Materials Chemistry B, 2(4) (2014), 363-375.

Mach, H., Middaugh, C. R., Lewis, R. V., Statistical determination of the average values of the extinction coefficients of tryptophan and tyrosine in native proteins, Analytical biochemistry, 200(1) (1992), 74-80.

Majorek, K. A., Porebski, P. J., Dayal, A., Zimmerman, M. D., Jablonska, K., Stewart, A. J., Chruszcz, M., Minor, W., Structural and immunologic characterization of bovine, horse, and rabbit serum albumins, Molecular Immunology, 52 (2012), 174-182.

Majumder, J. and Minko, T., Multifunctional and stimuli-responsive nanocarriers for targeted therapeutic delivery, Expert opinion on drug delivery, 18(2) (2021), 205-227.

Manju, S. and Sreenivasan, K., Conjugation of curcumin onto hyaluronic acid enhances its aqueous solubility and stability. Journal of colloid and interface science, 359(1) (2011), 318-325.

Meng, R., Zhu, H., Wang, Z., Hao, S., Wang, B., Preparation of drug-loaded albumin nanoparticles and its application in cancer therapy, Journal of Nanomaterials, (2022), 12 pages.

Mondal, M., Ramadas, K., Natarajan, S., Molecular interaction of 2, 4-diacetylphloroglucinol (DAPG) with human serum albumin (HSA): the spectroscopic, calorimetric and computational investigation, Spectrochimica Acta Part A: Molecular and Biomolecular Spectroscopy, 183 (2017), 90-102.

Mura, S., Nicolas, J., Couvreur, P., Stimuli-responsive nanocarriers for drug delivery, Nature materials, 12(11) (2013), 991-1003.

Murthy, M. S. R., and Sundaram, M. S., Spectrophotometric determination of dopamine hydrochloride, Indian journal of pharmaceutical sciences, 58(3) (1996), 124.

Onafuye, H., Pieper, S., Mulac, D., Cinatl Jr, J., Wass, M. N., Langer, K., & Michaelis, M., Doxorubicin-loaded human serum albumin nanoparticles overcome transporter-mediated drug resistance in drug-adapted cancer cells, Beilstein journal of nanotechnology, 10(1) (2019), 1707-1715.

Prajapati, R., Garcia-Garrido, E., Somoza, Á., Albumin-based nanoparticles for the delivery of doxorubicin in breast cancer, Cancers, 13(12) (2021), 3011.

Qiao, H., Sun, M., Su, Z., Xie, Y., Chen, M., Zong, L., Ping, Q., Kidney-specific drug delivery system for renal fibrosis based on coordination-driven assembly of catechol-derived chitosan, Biomaterials, 35(25) (2014), 7157-7171.

Sand, K. M. K., Bern, M., Nilsen, J., Noordzij, H. T., Sandlie, I., Andersen, J. T., Unraveling the interaction between FcRn and albumin: opportunities for design of albumin-based therapeutics, Frontiers in immunology, 682 (2015).

Schweigert, N., Zehnder, A. J., & Eggen, R. I., Chemical properties of catechols and their molecular modes of toxic action in cells, from microorganisms to mammals: minireview, Environmental microbiology, 3(2) (2001), 81-91.

Sever, M. J. and Wilker, J. J., Visible absorption spectra of metal–catecholate and metal–tironate complexes, Dalton Trans., (2004**)**, 1061-1072. .

Shalbafan, M., Rezaei Behbehani, G., Ghasemzadeh, H., Study of interaction of human serum albumin with doxorubicin (anti-cancer drug) by docking simulation, Chem. Methodol, 3(3) (2019), 276-391.

Shen, Y., Wang, B., Li, D., Yuan, W., Huang, Y., Hu, Z., Catechol-modified epoxy backbones for multifunctional and ultra-tough thermoset, Chemical Engineering Journal, 455 (2023), 140889.

Silverman, H. G. and Roberto, F. F., Understanding marine mussel adhesion, Marine biotechnology, 9 (2007), 661-681.

Singal, P. K. and Iliskovic, N., Doxorubicin-induced cardiomyopathy, The New England Journal of Medicine, 339 (13) (1998), 900–905.

Sombat K., Japrung D., Pongprayoon, P., Exploring how structural and dynamic properties of bovine and canine serum albumins differ from human serum albümin, Journal of Molecular Graphics and Modelling, 98 (2020), 107601.

Song, J., Lutz, T. M., Lang, N., Lieleg, O., Bioinspired dopamine/mucin coatings provide lubricity, wear protection, and cell-repellent properties for medical applications, Advanced Healthcare Materials, 10(4) (2021), 2000831.

Sozer, S. C., Akdogan, Y., Characterization of water solubility and binding of spin labeled drugs in the presence of albumin nanoparticles and proteins by electron paramagnetic resonance spectroscopy, ChemistrySelect, 7(6) (2022), e202103890.

Sozer, S. C., Egesoy, T. O., Basol, M., Cakan-Akdogan, G., Akdogan, Y., A simple desolvation method for production of cationic albumin nanoparticles with improved drug loading and cell uptake, Journal of Drug Delivery Science and Technology, 60 (2020), 101931.

Spada, A., Emami, J., Tuszynski, J. A., Lavasanifar, A., The uniqueness of albumin as a carrier in nanodrug delivery, Molecular Pharmaceutics, 18(5) (2021), 1862-1894.

Srivastava, A., and Prajapati, A., Albumin and functionalized albumin nanoparticles: Production strategies, characterization, and target indications. Asian Biomedicine, 14(6) (2020), 217-242.

Such, G. K. Yan, Y. Johnston, A. P. Gunawan, S. T. Caruso, F., Interfacing materials science and biology for drug carrier design, Adv. Mater., 27 (2015), 2278-2297.

Sugio, S., Kashima, A., Mochizuki, S., Noda, M., Kobayashi, K., Crystal structure of human serum albumin at 2.5 A resolution, Protein Engineering, 12 (1999), 439-446.

Sun, C., Lu, J., Wang, J., Hao, P., Li, C., Qi, L., Hao, N., Redox-sensitive polymeric micelles with aggregation-induced emission for bioimaging and delivery of anticancer drugs, Journal of Nanobiotechnology, 19(1) (2021), 1-15.

Sun, T., Zhang, Y. S., Pang, B., Hyun, D. C., Yang, M., Xia, Y., Engineered nanoparticles for drug delivery in cancer therapy, Angewandte Chemie International Edition, 53(46) (2014), 12320-12364.

Sundar, S., Kundu, J., Kundu, S. C., Biopolymeric nanoparticles, Science and Technology of Advanced Materials, 11(1) (2010), 014104.

Tatlidil, D., Ucuncu, M., & Akdogan, Y., Physiological concentrations of albumin favor drug binding, Physical Chemistry Chemical Physics, 17(35) (2015), 22678-22685.

Thorn, C. F., Oshiro, C., Marsh, S., Hernandez-Boussard, T., McLeod, H., Klein, T. E., Altman, R. B., Doxorubicin pathways: pharmacodynamics and adverse effects, Pharmacogenet. Genom. 21(7) (2011), 440–446.

Van Sluis, R., Bhujwalla, Z. M., Raghunand, N., Ballesteros, P., Alvarez, J., Cerdan, S., Galons, J. P., Gillies, R. J., In vivo imaging of extracellular pH using 1H MRSI. Magn. Reson. Med., 41 (1999), 743–750.

Verma, D., Gulati, N., Kaul, S., Mukherjee, S., Nagaich, U., Protein based nanostructures for drug delivery, Journal of pharmaceutics (2018).

Vismara, E., Bongio, C., Coletti, A., Edelman, R., Serafini, A., Mauri, M., Simonutti, R., Bertini, S., Urso, E., Assarag, Y. G., Livney, Y. D., Albumin and hyaluronic acid-coated superparamagnetic iron oxide nanoparticles loaded with paclitaxel for biomedical applications, Molecules, 22(7) (2017), 1030.

Vodyashkin, A. A., Kezimana, P., Vetcher, A. A., & Stanishevskiy, Y. M., Biopolymeric nanoparticles–multifunctional materials of the future. Polymers, 14(11) (2020), 2287.

Wei, W., Yu, J., Broomell, C., Israelachvili, J. N., Waite, J. H., Hydrophobic enhancement of dopa-mediated adhesion in a mussel foot protein, Journal of the American Chemical Society, 135(1) (2013), 377-383.

Xu, Z., Mechanics of metal-catecholate complexes: the roles of coordination state and metal types, Scientific reports, 3(1) (2013), 1-7.

Yang, H., Villani, R. M., Wang, H., Simpson, M. J., Roberts, M. S., Tang, M., Liang, X., The role of cellular reactive oxygen species in cancer chemotherapy, Journal of Experimental & Clinical Cancer Research, 37 (2018), 266.

Yang, Z., Zhang, N., Ma, T., Liu, L., Zhao, L., Xie, H., Engineered bovine serum albuminbased nanoparticles with pH-sensitivity for doxorubicin delivery and controlled release, Drug Deliv., 27 (01) (2020), 1156–1164.

Yen, G. C. and Hsieh, C. L., Antioxidant effects of dopamine and related compounds, Biosci. Biotechnol. Biochem., 61 (10) (1997), 1646-1649.

Yildiz, R., Ozen, S., Sahin, H., Akdogan, Y., The effect of DOPA hydroxyl groups on wet adhesion to polystyrene surface: An experimental and theoretical study, Materials Chemistry and Physics, 243 (2020), 122606.

Yoshida, T., Lai, T. C., Kwon, G. S., Sako, K., pH- and ion-sensitive polymers for drug delivery, Expert Opin. Drug Deliv., 10 (11) (2013), 1497–1513.

Zhang, J., Chen, L., Tse, W. H., Bi, R., Chen, L., Inorganic nanoparticles: engineering for biomedical applications, IEEE Nanotechnology Magazine, 8(4) (2014), 21-28.

Zhao, T., Huang, G., Li, Y., Yang, S. C., Ramezani, S., Lin, Z. Q., Wang, Y. G., Ma, X. P., Zeng, Z. Q., Luo, M., de Boer, E., Xie, X.-J., Thibodeaux, J., Brekken, R. A., Sun, X., Sumer, B. D., Gao, J., A transistor-like ph nanoprobe for tumour detection and image-guided surgery. Nat. Biomed. Eng. 1 (2017), 0006.

Zhu, W., Peck, Y., Iqbal, J., Wang, D. A., A novel DOPA-albumin based tissue adhesive for internal medical applications, Biomaterials, 147 (2017), 99-115.

Ziaaddini, V., Saeidifar, M., Eslami-Moghadam, M., Saberi, M., Mozafari, M., Improvement of efficacy and decrement cytotoxicity of oxaliplatin anticancer drug using bovine serum albumin nanoparticles: synthesis, characterization and release behavior, IET Nanobiotechnology, vol. 14, no. 1 (2020), pp. 105–111.